

Simulation of the gas-phase processes in remote-plasma-activated chemical-vapor deposition of silicon dielectrics using rare gas-silane-ammonia mixtures

Mark J. Kushner

University of Illinois, Department of Electrical and Computer Engineering, 1406 W. Green St., Urbana, Illinois 61801

(Received 17 September 1991; accepted for publication 17 January 1992)

Remote-plasma-activated chemical-vapor deposition (RPACVD) is a method whereby thin films are deposited with the substrate located out of the plasma zone. The lower rate of energetic ion and photon bombardment in RPACVD compared to conventional direct-plasma-enhanced chemical-vapor deposition (DPECVD) reduces damage to the substrate. The use of RPACVD also enables one to more carefully tailor the flux of radicals to the substrate compared to DPECVD. This selectivity results from both physically isolating the substrate from undesirable radicals and limiting the variety of chemical pathways that produce radicals. A model for RPACVD is described and results from the model are discussed in the context of comparing gas mixtures and geometries in which this selectivity may be achieved. The chemistries investigated are Rg/SiH_4 ($Rg = Ar, He$) for deposition of Si and $Rg/NH_3/SiH_4$ ($Rg = Ar, He$) for deposition of Si_3N_4 . It is found that the selectivity in producing radicals that can be obtained by excitation transfer from excited states of rare gases is easily compromised by reactor configurations that allow injected gases to penetrate into the plasma zone.

I. INTRODUCTION

Deposition of device quality silicon dielectric films (e.g., $a\text{-Si:H}$, SiO_2 , Si_3N_4) by plasma-enhanced chemical-vapor deposition (PECVD) is now standard practice in the fabrication of photovoltaics and very large-scale integrated-circuit (VLSIC) components.¹⁻³ The usual PECVD reactor consists of a parallel-plate capacitively coupled radio-frequency (rf) discharge. The commonly used pressures are from 100 mTorr to a few Torr with power depositions of tens to hundreds of $mW\text{ cm}^{-3}$. This results in plasma densities of $10^9\text{--}10^{10}\text{ cm}^{-3}$. In conventional PECVD reactors, the substrate or wafer sits on an electrode. It is therefore in contact with the plasma and subject to bombardment by energetic ions and photons. This mode of operation is described as direct-plasma-enhanced chemical-vapor deposition (DPECVD). The consequences of ion bombardment are varied. Ion bombardment of $a\text{-Si:H}$ films during deposition promotes columnar surface morphologies which result in poor electronic properties.⁴ Some amount of ion bombardment may, however, be beneficial in activating surface sites which promotes film growth and densifies the film. In rf diode discharges where ion energies can exceed hundreds of eV, the substrate is more likely to be damaged.⁵ This damage can be annealed in a later processing step. However, when fabricating microelectronics devices where the thermal budget must be minimized (e.g., metal-oxide-silicon gate structures) postdeposition annealing is undesirable.⁶

Another disadvantage of having the substrate in contact with the plasma is that the radical and ion fluxes that are incident on the substrate are difficult to control. These fluxes are generated by the nonselective excitation and dissociation of the feedstock gases by electron impact. The fragmentation is not selective because the electron-energy

distribution in typical rf diode reactors spans energies up to hundreds of eV.⁷ Therefore virtually all dissociation and excitation channels of the feedstock gases can be accessed. With these conditions it is difficult to control the plasma properties to a high enough degree to preferentially produce a flux of specific radicals to the substrate.

Remote-plasma-activated chemical-vapor deposition (RPACVD) is a process in which depositions are performed with the substrate located outside of the plasma zone.⁸⁻¹⁶ The immediate benefit is that the substrate is not subject to energetic ion bombardment. An added benefit is that one may also have more control over radical fluxes using RPACVD compared to DPECVD. Device quality silicon and silicon alloy films ($a\text{-Si:H}$, Si_3N_4 , SiO_2 , doped $\mu\text{-Si}$, epitaxial Si) have been produced using RPACVD by Lucovsky and Markunas⁸⁻¹³ and Tasch *et al.*¹⁴⁻¹⁶ In many cases the film properties obtained by RPACVD differed from those obtained from DPECVD using the same chemistry. For example, Parsons and co-workers⁹ found that SiO_2 and Si_3N_4 films obtained by DPECVD usually contained large fractions (5%–10%) of incorporated hydrogen in the form of NH and SiH. However, these bonding configurations were nearly absent in films deposited by RPACVD.

There are two variants of RPACVD reactors (see Fig. 1). In the first variant, deposition gases pass through an isolated plasma zone and flow to a substrate located downstream. Charged particles are largely confined to and near the upstream plasma zone, resulting in a flux of mostly neutral radicals to the substrate. In the second variant, nondeposition gases (or a subset of the required deposition gases) are flowed through the plasma zone. Plasma-activated neutral atoms and radicals flow downstream where (additional) deposition gases are injected. Excitation

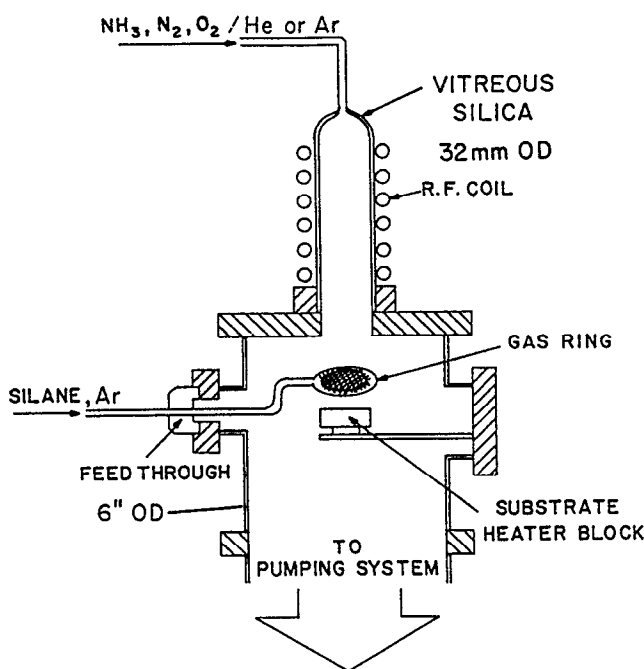


FIG. 1. Schematic of experimental RPACVD reactor. The plasma is sustained in the narrow tube at the top. Nondeposition gases, or a subset of the required deposition gases, are flowed through the plasma zone and into the lower mixing chamber. Additional deposition gases are injected through dispersal rings in the lower chamber (from Ref. 8).

transfer reactions between the activated neutrals and the deposition gases produce the deposition precursors which are transported to the substrate. For example, the deposition of Si_3N_4 by RPACVD can be accomplished by flowing He/N_2 or He/NH_3 mixtures through the plasma zone, and injecting SiH_4 downstream.⁸

One of the advantages of RPACVD is the improved capability to control the radicals that are incident on the substrate. This is accomplished by either physically or chemically isolating the substrate. For example, consider the RPACVD of a silicon alloy in which silane is the feedstock. For purposes of discussion, assume that Si atom radicals are not desirable in the flux to the substrate. If silane is flowed through the plasma zone, Si atoms will be produced by electron-impact dissociation. One must then rely upon physical isolation to eliminate Si atoms from the radical flux. This is accomplished by locating the substrate far enough downstream so that diffusion to the walls or gas-phase reactions deplete the flux of Si atoms before reaching the substrate. In chemical isolation, Si atoms are eliminated from the radical flux by selecting a radical production method in which Si atoms are simply not formed in abundance. For example, this can be accomplished by flowing H_2 through the plasma zone and injecting SiH_4 downstream. H atoms produced in the plasma will abstract H from SiH_4 , generating SiH_3 as the primary product. Si atoms are not directly produced.

The absence of ion bombardment in RPACVD may allow the use of gas mixtures that produce more favorable

radical fluxes. For example, DPECVD using Rg/SiH_4 mixtures (Rg = rare gas) usually results in poor film properties due to ion bombardment which causes columnar structure.⁴ In RPACVD, where energetic ion bombardment is not important, lean Rg/SiH_4 mixtures can be used.¹⁰ These lean mixtures tend to minimize the amount of plasma polymerization that occurs and results in incorporation of primarily mono-silane radicals into the film.¹⁷

In this paper, a model for the electron kinetics and plasma chemistry in the RPACVD of Si alloys is described. The model is a two-dimensional description of the generation and transport of plasma-activated species. Results will be discussed for RPACVD with Rg/SiH_4 and $\text{Rg}/\text{SiH}_4/\text{NH}_3$ mixtures as used in the deposition of $\mu\text{c-Si}$, $\alpha\text{-Si:H}$, and Si_3N_4 . We find that when the injected SiH_4 is isolated from the plasma zone, the flux of radicals to the substrate can be controlled by using different activation gases (e.g., He, Ar). This control stems from the different dissociative excitation patterns resulting from excitation transfer from ions and excited states of the rare gases. The flux of radicals to the substrate can be partly controlled by flow rate and placement of injection nozzles, since these parameters determine the degree to which the injected gases are isolated from the plasma. However, at low pressures (\leq hundreds of mTorr) and moderate residence times ($>$ tens of ms), the back diffusion of injected gases into the plasma zone is primarily responsible for generating radicals. In that case, physical isolation provides the means to selectively produce radical fluxes. The model is described in Sec. II where the plasma chemistry of $\text{Rg}/\text{SiH}_4/\text{NH}_3$ mixtures is also discussed. Results from the model are presented in Sec. III followed by concluding remarks in Sec. IV.

II. DESCRIPTION OF THE MODEL AND REACTION MECHANISMS

Our model for RPACVD simulates a cylindrical reactor of the type schematically shown in Fig. 1. The gas pressure is 100–200 mTorr and flow rates are many hundreds of sccm resulting in residence times of tens to hundreds of ms. Gases flow into the reactor through a narrow tube where the plasma is sustained by a capacitively coupled rf discharge. The activated inlet gases flow downstream where (additional) deposition gases are injected through circular nozzles. The model consists of two coupled simulations for the electron kinetics and plasma chemistry. The former model is used to generate electron-impact rate coefficients which are used in the latter model. The rate coefficients are obtained from a Monte Carlo simulation for the electron kinetics and therefore reflect the nonequilibrium nature of the electron-energy distribution in the plasma. Conceptually, the full model consists of modules for electron kinetics, transport, and plasma chemistry. The species included in the model are listed in Table I.

A. Electron kinetics

The electron kinetics in and downstream of the plasma zone are simulated in similar fashion to the model de-

TABLE I. Species used in the model.

Rare gases and electrons						
He	He*	He ⁺				
Ar	Ar*	Ar ⁺	ArH ⁺	<i>e</i>		
Hydrogen species						
H ₂	H ₂ ⁺	H ₃ ⁺	H	H ⁺	H ⁻	
Silane species						
SiH ₄	SiH ₄ (<i>v</i> 1,3)	SiH ₄ (<i>v</i> 2,4)	Si ₂ H ₆	Si ₃ H ₈	Si ₄ H ₁₀	Si ₅ H ₁₂
Si	SiH	SiH ₂	SiH ₃			
Si ₂ H ₂	Si ₂ H ₃	Si ₂ H ₄	Si ₂ H ₅	Si ₃ H ₇	Si ₄ H ₉	Si ₅ H ₁₁
SiH ₃ ⁺	SiH ₂ ⁺	SiH ⁺	Si ⁺			
Si ₂ H ₇ ⁺	Si ₂ H ₅ ⁺	Si ₂ H ₄ ⁺	Si ₂ H ₃ ⁺	Si ₂ H ₂ ⁺	Si ₃ H ₄ ⁺	
Si ₃ H ₆ ⁺	Si ₃ H ₇ ⁺	Si ₃ H ₉ ⁺	Si ₄ H ₆ ⁺	Si ₄ H ₈ ⁺	Si ₄ H ₁₁ ⁺	Si ₅ H ₁₀ ⁺
SiH ₄ N ⁺	SiH ₃ N ⁺	SiH ₂ N ⁺	SiH ₂ ⁻	SiH ₃ ⁻		
Ammonia species						
NH ₃	NH ₃	NH	N	N ₂		
NNH	N ₂ H ₂	N ₂ H ₄				
NH ₂ ⁺	NH ₃ ⁺	NH ₄ ⁺				
Amino-silane complexes						
SiH ₂ (NH ₂)	SiH(NH ₂) ₂	Si(NH ₂) ₃				
SiH ₃ (NH ₂)	SiH ₂ (NH ₂) ₂	SiH(NH ₂) ₃	Si(NH ₂) ₄			

scribed in Ref. 18 for PECVD of *a*-Si:H in a capacitively coupled parallel-plate radio-frequency discharge. The electron kinetics model is a Monte Carlo simulation (MCS) that follows the trajectories of electron pseudoparticles in specified electric fields. The MCS is separately run to generate electron-impact rate coefficients as a function of position which are then used as input to the plasma chemistry model. The MCS, which is also described in Refs. 19 and 20, includes complete sets of experimental electron-impact cross sections for all species of interest (Ar, He, H₂, NH₃, SiH₄, Si₂H₆). Cross sections for SiH₄ and Si₂H₆ used in the model are described in Ref. 18. Those for NH₃, He, and Ar were obtained from Refs. 21, 22, and 23, respectively.

The MCS is run over many rf cycles until the electron-energy distribution converges to a quasisteady state. Electron-impact rate coefficients are computed from the time-averaged electron-energy distribution and parameterized as a function of voltage and the electric field in the bulk plasma. In the plasma chemistry model, a power deposition is specified for the upstream plasma zone. The values of the rate coefficients from the MCS are interpolated as a function of bulk electric field while integrating the species continuity equations until a self-consistent quasi-steady-state plasma at the specified power deposition is obtained. The axial extent over which the plasma is externally sustained is specified as input to the plasma chemistry model. In the results discussed here the plasma is restricted to the narrow portion of the reactor.

B. Transport

Fully two- and three-dimensional flow models for thermal and plasma CVD have been presented in both the literature and are available as commercial products. Applying those models to RPACVD is difficult due to the

large number of species and reactions, and the very disparate time scales required to model processes in the upstream plasma zone and the downstream reaction chamber. We have, therefore, simplified the transport model in our simulation. We assume that in spite of the low pressures of interest (\leq hundreds of mTorr) the continuum formulation for transport is valid and the flow is isothermal. This is a marginal assumption since the Knudsen number is approximately 0.01. We further assume that transport of all heavy particle species can be described by the same advective velocity. Since electron transport is constrained by ambipolar forces, electron transport mirrors that of the heavy ions. The advective flow field is obtained by solving modified transport equations for ideal flow (viscosity $\mu = 0$),²⁴

$$\frac{\partial \rho \mathbf{v}}{\partial t} = -\nabla \cdot \rho \mathbf{v} \frac{\phi}{N} - \nabla P, \quad \frac{\partial N}{\partial t} = -\nabla \cdot \phi, \quad (1)$$

where \mathbf{v} is the advective velocity, N is the gas density, and $\rho = NM$ is the mass density for average molecular weight M , and $P = NkT$ is the thermodynamic pressure for temperature T . The total convective particle flux (including diffusion) is $\phi = N\mathbf{v} - D\nabla N$, where D is the average diffusion coefficient. This form of the flux is used in the momentum equation to approximate the diffusive nature of the flow. The injected gases are assumed to instantaneously take on the advective velocity of the local flow field. As a practical matter, the advective flow field is separately calculated in the model. The radial and axial advective velocities are then stored for use in the transport portion of the plasma kinetics.

The conservation equation solved for species i having density N_i is

$$\frac{\partial N_i}{\partial t} = -\nabla \cdot (\mathbf{v}N_i - D_i \nabla N_i) \pm \sum N_j N_l k_{jl} \quad (2)$$

where \mathbf{v} is the advective velocity described above, D_i is the diffusion coefficient, and k_{jl} is a rate coefficient for reactions between species j and l . The local reaction kinetics are discussed in the following section. The boundary conditions on the axis are $(\partial N_i / \partial r)_{r=0} = 0$. The boundary conditions at the wall depend on the sticking and reaction coefficients of the particular species of interest. In practice, this is accomplished by generating an array of reaction probabilities p_{ij} , which is the probability that species i diffusing to the wall "returns" as species j . For a nonreacting species, $p_{ii} = 1$, whereas $p_{ij \neq i} = 0$. For a monomer species that reacts with unity probability at the wall returning only as a dimer species (for example, $2\text{H} \rightarrow \text{wall} \rightarrow \text{H}_2$) we have $p_{11} = 0$ and $p_{12} = 0.5$. The p_{ij} may be functions of position, temperature, surface coverage, or other conditions. The boundary condition for the flux of species i returning to the plasma ϕ_{ir} based on fluxes to the wall ϕ_i is then $\phi_{ir} = \sum p_{ij} \phi_j$. The same method was used to specify fluxes to and from vertical surfaces in the axial direction.

The time steps that are required for numerical stability when integrating the plasma kinetic rate equations are usually small compared to those required for numerical stability when integrating the transport equations. The transport and plasma kinetics portions of the continuity equations are therefore separately integrated using a time slicing technique. The densities of all species are updated based only on local kinetics for many kinetic time steps Δt_K followed by a transport update with timestep Δt_T . The ratio of time steps is usually $1 < \Delta t_T / \Delta t_K < 20$. The kinetic time step is chosen dynamically at each mesh point and the densities at each mesh point are separately updated until the local time has been advanced by Δt_T . In this manner the shorter time steps required in the plasma zone do not constrain the calculation at mesh points further downstream. The transport update is then uniformly applied across the entire mesh. All updates are performed using a third-order Runge-Kutta technique.

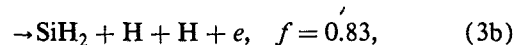
C. Plasma kinetics: Silane

The reaction scheme for Ar/SiH₄ gas mixtures used in the model is basically the same as that described in Ref. 18. Since the time of that work, however, additional experimental measurements have become available or become known. A subset of the rate coefficients and transport coefficients described in Ref. 18 has therefore been updated. Those values will be briefly discussed.

The Lennard-Jones parameters used for calculating neutral transport coefficients for Si_{*n*}H_{*m*} molecules and radicals have been revised to conform to those of Coltrin, Kee, and Evans.²⁵ Lennard-Jones parameters for other species were updated to conform to those given in Ref. 26.

The branching ratio for electron-impact dissociation of SiH₄ into neutral fragments has still not been directly measured. However, Doughty and Gallagher²⁷ recently spatially resolved the deposition rate of α -Si:H in a rf silane

plasma. Their analysis of the results strongly suggests that the dominant fragments in the neutral dissociation of silane are SiH₂ + 2H. In view of these findings, our branchings for neutral electron-impact dissociation of silane have been revised to



where f denotes the branching ratio. The branching for dissociative ionization are given by the convolution of the electron-energy distribution with their respective cross sections as in the previous work.¹⁸ The only revision to previous values is that the hydrogen produced in the branching to SiH₂⁺ is now 2H instead of H₂, in analogy to that for the neutral branchings.

Association reactions often proceed through an intermediate state which must be collisionally stabilized. In the absence of these stabilizing collisions, the complex may dissociate back into its original reactants or other fragments. At the gas pressures of interest (< 1 Torr), many association reactions are in the "falloff regime" in which their effective two-body rate coefficients decrease with decreasing gas pressure due to the lack of stabilizing collision partners. Recent measurements by Jasinski *et al.*^{28,29} have yielded rate coefficients as a function of gas pressure for SiH₂ reacting with SiH₄ and H₂, and for SiH₃ reacting with SiH₃. Those pressure-dependent values have been used in this study.

Definitive works on charge-exchange cross sections of positive silane ions with silane by Haaland³⁰ and Mandich *et al.*³¹⁻³³ have shown the possibility of bottlenecks in the formation of higher-order clusters. Specifically, sequential ion-molecule reactions of Si⁺ and SiH₃⁺ with silane generate higher-order silane ions as large as Si₆H_{*n*}⁺. Further reactions with silane, however, have activation barriers which at thermal energies constitute bottlenecks in the reaction chain. Updated rate coefficients for charge transfer reaction of silane ions, which include these new findings, were included in the model and are shown in Table II. Many of the original measurements were made with deuterated species for purposes of species discrimination. Those values were used for hydrogenated species without further adjustment. Table II is less inclusive than the reaction scheme described in Ref. 18 for two reasons. The first is the mentioned bottlenecking reactions in the ion clustering sequence which prevents the formation of some higher-order silane ions. The second is that the ion energies in RPACVD are significantly less than the energies of ions in the sheaths of DPECVD rf diodes. Therefore, charge-exchange reactions which are endothermic at thermal energies and might occur in the sheaths of DPECVD reactors are unimportant in RPACVD.

Dissociative charge- and excitation-transfer reactions between Ar*, Ar⁺, He*, and He⁺, and the deposition gases form the basis of highly selective RPECVD. The differences in branchings for these processes compared to direct electron-impact dissociation may be largely responsible for the differences in film properties found in

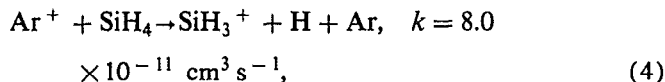
TABLE II. Ion-molecule reactions with silane.

Reaction	Rate coefficient ^a	Ref.
$\text{SiH}_3^+ + \text{SiH}_4 \rightarrow \text{Si}_2\text{H}_3^+ + \text{H}_2 + \text{H}_2$	1.00×10^{-14}	31
$\text{SiH}_3^+ + \text{SiH}_4 \rightarrow \text{Si}_2\text{H}_5^+ + \text{H}_2$	2.80×10^{-11}	31
$\text{SiH}_3^+ + \text{SiH}_4 + \text{M} \rightarrow \text{Si}_2\text{H}_7^+ + \text{M}$	1.80×10^{-25}	b,31
$\text{SiH}_2^+ + \text{SiH}_4 \rightarrow \text{SiH}_3^+ + \text{SiH}_3$	1.07×10^{-9}	51
$\text{SiH}_2^+ + \text{SiH}_4 \rightarrow \text{Si}_2\text{H}_2^+ + \text{H}_2 + \text{H}_2$	5.50×10^{-11}	51
$\text{SiH}_2^+ + \text{SiH}_4 \rightarrow \text{Si}_2\text{H}_4^+ + \text{H}_2$	2.50×10^{-10}	51,52
$\text{SiH}^+ + \text{SiH}_4 \rightarrow \text{SiH}_3^+ + \text{SiH}_2$	5.98×10^{-10}	30
$\text{SiH}^+ + \text{SiH}_4 \rightarrow \text{SiH}_2^+ + \text{SiH}_3$	1.95×10^{-10}	30
$\text{SiH}^+ + \text{SiH}_4 \rightarrow \text{Si}_2\text{H}_3^+ + \text{H}_2$	5.07×10^{-10}	30
$\text{SiH}^+ + \text{SiH}_4 + \text{M} \rightarrow \text{Si}_2\text{H}_5^+ + \text{M}$	1.30×10^{-26}	53
$\text{Si}^+ + \text{SiH}_4 \rightarrow \text{SiH}_3^+ + \text{H}$	6.50×10^{-10}	30,31
$\text{Si}^+ + \text{SiH}_4 \rightarrow \text{SiH}_2^+ + \text{H}_2$	2.20×10^{-10}	30,31
$\text{Si}^+ + \text{SiH}_4 \rightarrow \text{SiH}^+ + \text{H} + \text{H}_2$	2.20×10^{-10}	30,31
$\text{Si}^+ + \text{SiH}_4 \rightarrow \text{Si}_2\text{H}_2^+ + \text{H}_2$	2.20×10^{-10}	30,31
$\text{Si}^+ + \text{SiH}_4 + \text{M} \rightarrow \text{Si}_2\text{H}_4^+ + \text{M}$	1.40×10^{-26}	53
$\text{Si}_2\text{H}_3^+ + \text{SiH}_4 \rightarrow \text{Si}_3\text{H}_6^+ + \text{H}$	5.00×10^{-11}	52,53
$\text{Si}_2\text{H}_4^+ + \text{SiH}_4 \rightarrow \text{Si}_3\text{H}_6^+ + \text{H}_2$	5.20×10^{-11}	52,53
$\text{Si}_2\text{H}_5^+ + \text{SiH}_4 + \text{M} \rightarrow \text{Si}_3\text{H}_9^+ + \text{M}$	1.00×10^{-26}	b,32
$\text{Si}_2\text{H}_6^+ + \text{SiH}_4 \rightarrow \text{Si}_3\text{H}_6^+ + \text{H}_2 + \text{H}_2$	5.00×10^{-11}	52,53
$\text{Si}_2\text{H}_7^+ + \text{SiH}_4 + \text{M} \rightarrow \text{Si}_4\text{H}_{11}^+ + \text{M}$	1.00×10^{-26}	b,32
$\text{Si}_3\text{H}_4^+ + \text{SiH}_4 \rightarrow \text{Si}_4\text{H}_6^+$	1.74×10^{-10}	32
$\text{Si}_4\text{H}_6^+ + \text{SiH}_4 \rightarrow \text{Si}_5\text{H}_{10}^+$	1.00×10^{-13}	32

^aRate coefficients have units of $\text{cm}^3 \text{s}^{-1}$ unless noted.

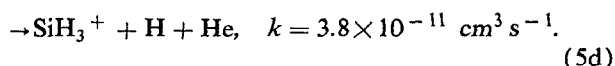
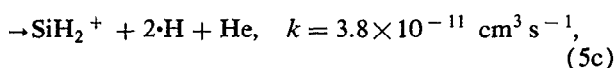
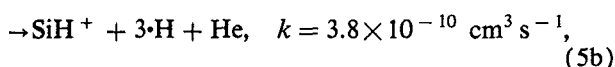
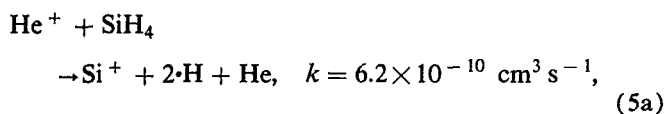
^bThe value used in the model is lower than that quoted in the cited reference for computational reasons. Due to the large value of either rate coefficient, there is no significant change in the resulting kinetics.

DPECVD and RPACVD, and between RPACVD films produced using different activation gases. Fisher and Armentrout³⁴ and Haaland³⁰ have shown that the charge-exchange reaction of Ar^+ with silane at thermal energies has only a single significant branching,



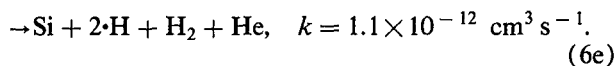
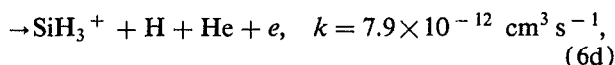
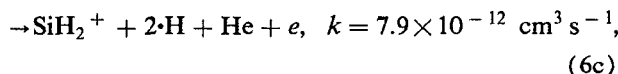
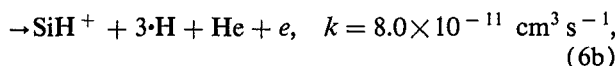
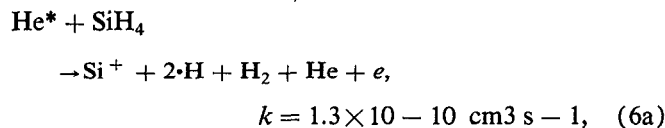
where k is the rate coefficient for the process. This revised branching is used in the model.

The charge exchange of He^+ with SiH_4 dominantly forms Si^+ and SiH^+ , though the neutral fragments have not been measured. The exothermicity of the process allows any fragmentation pattern, including excited states of the fragments. Steric factors lead one to conclude that dissociations that result in forming H_2 as a fragment are less likely than those forming 2H . We used the experimental results of Chatham *et al.*,³⁵ Fisher and Armentrout,³⁴ and Haaland³⁰ for total-reaction rate coefficients and for branching of the ion fragments in the model. Branchings for neutrals were estimated. The final reaction scheme is



It is interesting to note that these branchings significantly differ from those for electron-impact ionization of silane by a 25 eV electron, the potential energy of He^+ . Measurements by Chatham *et al.*³⁶ for electron-impact ionization have major branchings to SiH_2^+ and SiH_3^+ . Since the dissociation following electron impact most likely results from a vertical transition to a dissociative electronic state, one may conclude that the charge-exchange reactions access other states, presumably corresponding to a different equilibrium separation.

The branchings for dissociative excitation transfer of $\text{Ar}(4s)$ and $\text{He}(2^3S, 2^1S)$ with silane are less well known. The total rate coefficient for quenching of excited states of He by silane has been measured by Yoshida *et al.*³⁷ to be $2.3 \times 10^{-10} \text{ cm}^3 \text{ s}^{-1}$. They conclude that virtually all of the fragments are charged. Neutral excited Si fragments have, however, been observed by Tsuji *et al.*³⁸ and are produced with a rate coefficient of $1.1 \times 10^{-12} \text{ cm}^3 \text{ s}^{-1}$. In assigning branchings to the dissociative quenching of He^* by SiH_4 , one must choose between a reaction resulting in a vertical electronic transition, as in electron impact, or a transition that is analogous to the charge-transfer reaction. The latter branching was chosen. However, since the metastable states of He have an energy approximately 5 eV lower than that of the ion, certain branchings of neutral products that are obtained in the charge-exchange reaction are not energetically allowed in metastable quenching. With those considerations, the branchings and rate coefficients for quenching of He^* by SiH_4 used in the model are



The rate coefficient for the quenching of $\text{Ar}(4s)$ by SiH_4 has been measured Tsuji *et al.*³⁹ and Joubertau *et al.*⁴⁰ The values obtained are $4.8\text{--}6.0 \times 10^{-10} \text{ cm}^3 \text{ s}^{-1}$. The branchings of the silane products have not been completely measured. Tsuji *et al.* determined that quenching resulted in excited states of Si and SiH with branchings of 0.04 and 0.003, respectively.³⁹ The remaining branchings were estimated to be either SiH_2 or SiH_3 . The energy of excited states of argon could allow dissociative Penning ionizations with silane. A Penning reaction with $\text{Ar}(4s)$ resulting in $\text{SiH}_2^+ + \text{H}_2$ is endothermic by only 0.09 eV and would be directly assessable to higher excited states of Ar. In particular, the reaction with $\text{Ar}(4s')$ would be exothermic by

TABLE III. Ammonia-silane reactions used in the model.^a

Reaction	Rate coefficient ^b	Ref.
NH_x reactions		
NH ₃ + H → H ₂ + NH ₂	$1.34 \times 10^{-10} \exp(-7325/T_g)$	54
NH ₃ + NH + M → N ₂ H ₄ + M	$5.00 \times 10^{-35} \text{ cm}^6 \text{ s}^{-1}$	55
NH ₂ + H → NH + H ₂	4.81×10^{-12}	56
NH ₂ + H + M → NH ₃ + M	$6.06 \times 10^{-30} \text{ cm}^6 \text{ s}^{-1}$	57
NH ₂ + H ₂ → H + NH ₃	$2.09 \times 10^{-12} \exp(-4277/T_g)$	58
NH ₂ + NH ₂ + M → N ₂ H ₄ + M	$6.90 \times 10^{-30} \text{ cm}^6 \text{ s}^{-1}$	59
NH ₂ + NH ₂ → N ₂ H ₂ + H ₂	8.31×10^{-11}	41
NH ₂ + NH ₂ → NH ₃ + NH	$8.31 \times 10^{-11} \exp(-5100/T_g)$	41
NH ₂ + N → N ₂ + H + H	1.20×10^{-10}	41
NH ₂ + NH → N ₂ H ₂ + H	$2.49 \times 10^{-9} (T_g^{-1/2})$	41
NH + H ₂ → H + NH ₂	$5.96 \times 10^{-11} \exp(-7782/T_g)$	60
NH + H → H ₂ + N	$5.98 \times 10^{-11} \exp(-166/T_g)$	41
NH + H + M → NH ₂ + M	$8.72 \times 10^{-25} (T_g^{-2}) \text{ cm}^6 \text{ s}^{-1}$	41
NH + N → N ₂ + H	4.98×10^{-11}	41
NH + NH → N ₂ + H + H	8.31×10^{-11}	41
N + H + M → NH + M	$5.00 \times 10^{-32} \text{ cm}^6 \text{ s}^{-1}$	61
N ₂ H ₂ + H → NNH + H ₂	$8.31 \times 10^{-11} \exp(-510/T_g)$	41
N ₂ H ₂ + NH → NNH + NH ₂	$1.66 \times 10^{-11} \exp(-510/T_g)$	41
N ₂ H ₂ + NH ₂ → NNH + NH ₃	$1.66 \times 10^{-11} \exp(-510/T_g)$	41
NNH + H → N ₂ + H ₂	$6.64 \times 10^{-11} \exp(-1531/T_g)$	41
NNH + NH → N ₂ + NH ₂	8.30×10^{-11}	41
NNH + NH ₂ → N ₂ + NH ₃	8.30×10^{-11}	41
NH_x-SiH_x reactions		
NH ₂ + SiH ₄ → NH ₃ + SiH ₃	8.00×10^{-14}	29
NH ₂ + SiH ₃ → SiH ₂ NH ₂ + H	1.00×10^{-10}	29
NH ₂ + SiH ₂ NH ₂ → SiH(NH ₂) ₂ + H	1.00×10^{-10}	29
NH ₂ + SiH(NH ₂) ₂ → Si(NH ₂) ₃ + H	1.00×10^{-10}	29
NH ₂ + Si(NH ₂) ₃ → Si(NH ₂) ₄	1.00×10^{-10}	29
H + SiH ₂ NH ₂ → SiH ₃ NH ₂	1.70×10^{-11}	29
H + SiH(NH ₂) ₂ → SiH ₂ (NH ₂) ₂	5.00×10^{-11}	29
H + Si(NH ₂) ₃ → SiH(NH ₂) ₃	1.00×10^{-10}	29
H + SiH ₃ NH ₂ → SiH ₂ NH ₂ + H ₂	5.00×10^{-11}	c
H + SiH ₂ (NH ₂) ₂ → SiH(NH ₂) ₂ + H ₂	5.00×10^{-11}	c
H + SiH(NH ₂) ₃ → Si(NH ₂) ₃ + H ₂	5.00×10^{-11}	c
NH + SiH ₄ → SiH ₂ NH ₂ + H	1.00×10^{-11}	c
NH + SiH ₃ → SiH ₂ NH ₂	5.00×10^{-11}	c
NH ₂ + SiH ₂ → SiH ₂ NH ₂	5.00×10^{-11}	c
NNH + SiH ₄ → N ₂ + H ₂ + SiH ₃	1.00×10^{-13}	c
NNH + SiH ₃ → SiH ₄ + N ₂	5.00×10^{-11}	c
NNH + SiH ₂ → SiH ₃ + N ₂	5.00×10^{-11}	c
NNH + SiH → SiH ₂ + NH	5.00×10^{-11}	c
SiH ₂ + NH ₃ → SiH ₃ NH ₂	1.00×10^{-13}	c
Excitation transfer and ion-molecule reactions		
Ar ⁺ + NH ₃ → NH ₃ ⁺ + Ar	1.30×10^{-9}	43
Ar* + NH ₃ → NH ₃ ⁺ + Ar + e	4.20×10^{-11}	62,d
Ar* + NH ₃ → NH ₂ + H + Ar	5.80×10^{-11}	62,d
He ⁺ + NH ₃ → NH ₂ ⁺ + H + He	1.15×10^{-9}	43
He ⁺ + NH ₃ → NH ₃ ⁺ + He	5.00×10^{-10}	43
He ⁺ + NH ₃ → NH ₃ ⁺ + He	5.00×10^{-10}	43
He* + NH ₃ → NH ₃ ⁺ + He + e	4.15×10^{-10}	63,e
He* + NH ₃ → NH ₂ ⁺ + H + He + e	1.80×10^{-10}	63,e
SiH ₃ ⁺ + NH ₃ → SiH ₄ N ⁺ + H ₂	3.00×10^{-10}	44
SiH ₃ ⁺ + NH ₃ → NH ₄ ⁺ + SiH ₂	2.50×10^{-10}	44
SiH ₂ ⁺ + NH ₃ → SiH ₄ N ⁺ + H	4.60×10^{-10}	44
SiH ₂ ⁺ + NH ₃ → SiH ₃ N ⁺ + H ₂	1.30×10^{-10}	44
SiH ₂ ⁺ + NH ₃ → NH ₄ ⁺ + SiH	0.66×10^{-10}	44
SiH ⁺ + NH ₃ → SiH ₂ N ⁺ + H ₂	1.08×10^{-10}	44
SiH ⁺ + NH ₃ → SiH ₄ N ⁺	5.40×10^{-11}	44
SiH ⁺ + NH ₃ → NH ₄ ⁺ + Si	1.80×10^{-11}	44
NH ₃ ⁺ + SiH ₄ → NH ₄ ⁺ + SiH ₃	2.64×10^{-9}	44
NH ₃ ⁺ + SiH ₄ → SiH ₃ ⁺ + NH ₂ + H ₂	9.54×10^{-10}	44

TABLE III. (Continued.)

Reaction	Rate coefficient ^b	Ref.
$\text{NH}_2^+ + \text{SiH}_4 \rightarrow \text{NH}_3^+ + \text{NH}_2$	1.0×10^{-9}	c
$\text{SiH}_3\text{N}^+ + \text{NH}_3 \rightarrow \text{SiH}_4\text{N}^+ + \text{NH}_2$	6.36×10^{-10}	44
$\text{SiH}_2\text{N}^+ + \text{NH}_3 \rightarrow \text{SiH}_3\text{N}^+ + \text{NH}_2$	2.50×10^{-10}	44,c
$\text{NH}_3^+ + \text{NH}_3 \rightarrow \text{NH}_4^+ + \text{NH}_2$	2.20×10^{-9}	43
$\text{NH}_3^+ + \text{H}_2 \rightarrow \text{NH}_4^+ + \text{H}$	4.00×10^{-13}	43
$\text{NH}_2^+ + \text{H}_2 \rightarrow \text{NH}_3^+ + \text{H}$	1.00×10^{-9}	43
Electron impact		
$e + \text{NH}_2^+ \rightarrow \text{NH} + \text{H}$	g	c
$e + \text{NH}_3^+ \rightarrow \text{NH}_2 + \text{H}$	g	c
$e + \text{NH}_4^+ \rightarrow \text{NH}_3 + \text{H}$	g	42,f
$e + \text{SiH}_4\text{N}^+ \rightarrow \text{SiH} + \text{NH}_3$	g	c
$e + \text{SiH}_3\text{N}^+ \rightarrow \text{SiH} + \text{NH}_2$	g	c
$e + \text{SiH}_2\text{N}^+ \rightarrow \text{SiH} + \text{NH}$	g	c
$e + \text{NH}_3 \rightarrow \text{NH}_2 + \text{H}^-$	g	21
$e + \text{NH}_3 \rightarrow \text{NH}_2 + \text{H} + e$	g	21
$e + \text{NH}_3 \rightarrow \text{NH} + \text{H} + \text{H} + e$	g	21
$e + \text{NH}_3 \rightarrow \text{NH}_3^+ + e + e$	g	21,64
$e + \text{NH}_3 \rightarrow \text{NH}_2^+ + \text{H} + e + e$	g	21,64
$e + \text{NH}_2 \rightarrow \text{NH} + \text{H} + e$	g	21,42
$e + \text{NH}_2 \rightarrow \text{NH}_2^+ + e + e$	g	21,42

^aA detailed listing of rate coefficients for silane-hydrogen plasma chemistry can be found in Ref. 18. Modifications to this reaction scheme are discussed in Sec. II C.

^bRate coefficients have units of $\text{cm}^3 \text{s}^{-1}$ unless noted. T_g is the gas temperature (K).

^cEstimated. See the text for discussion.

^dTotal rate coefficient for Ar^* quenching by NH_3 was estimated. Branching ratios were obtained from Ref. 63.

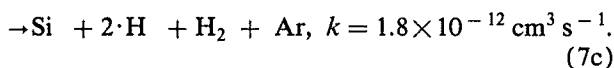
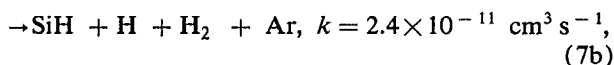
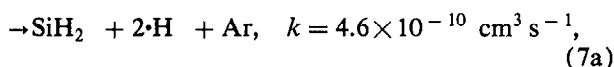
^eBranchings for He^* quenching by NH_3 were estimated. See text for discussion.

^fRate coefficient was estimated. Branching is as recommended by Ref. 42.

^gRate coefficient was obtained by convolving the electron-energy distribution with the cross section from the indicated reference.

0.09 eV. Since, however, even at 0.1 Torr the rate of collisional relaxation of $\text{Ar}(4s') \rightarrow \text{Ar}(4s)$ is high, we have assumed that the ion channel is not important and have specified that there be only neutral fragments. Our estimates for branchings are

$\text{Ar}^* + \text{SiH}_4$

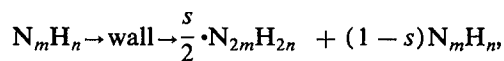


D. Plasma kinetics: Ammonia

The reaction chemistry of ammonia fragments has been previously investigated in the context of pyrolysis of ammonia⁴¹ and its radiation chemistry.⁴² The reaction scheme involving ammonia and its fragments used in the model appears in Table III. In the low-pressure and low-temperature limit, NH and NH_2 radicals are fairly unreactive with NH_3 . Ammonia neutral chemistry at low pressures (< 1 Torr) and temperatures of less than 500 K is therefore dominated by wall reactions and radical-radical reactions. Reactions of NH with H produces N_2 and H_2 with nearly equal branchings, whereas NH reactions with other NH radicals form $\text{N}_2 + 2\text{H}$. The end result is that NH fragments evolve dominantly to N_2 and H_2 . NH_2 frag-

ments mutually react to form N_2H_2 , react with H to form NH, and react with NH to form N_2H_2 . N_2H_2 in turn reacts with H to form NNH. The end result is that NH_2 fragments evolve towards N_2 , N_2H_2 , and NNH, the latter of which is slowly converted to $\text{N}_2 + \text{H}_2$ in the presence of H.

The degree to which low-pressure ammonia chemistry is dominated by wall reactions depends on the details of the surface reaction coefficients. To demonstrate this dependency in our geometry, the following computer experiment was performed. Mixtures of $\text{NH}_3/\text{NH}/\text{H} = 99.7/0.1/0.2$ and $\text{NH}_3/\text{NH}_2/\text{H} = 99.8/0.1/0.1$ at 0.2 Torr, as might result from electron-impact dissociation, were passed through a cylindrical vessel (radius 4 cm) for a residence time of 30 ms. Wall reactions were either ignored or included in the calculation with probabilities s of 0.10 and 0.01. The wall reactions we specified were



$$0 < m < 1, \quad 0 < n < 2. \quad (8)$$

The results of the computer experiments are shown in Fig. 2. In the $\text{NH}_3/\text{NH}/\text{H}$ mixture, production of N_2H_2 and N_2H_4 are dominated by wall reactions while that of H_2 is not sensitive to the wall reactions. Production of N_2 has an intermediate sensitivity. In the $\text{NH}_3/\text{NH}_2/\text{H}$ system, only the production of N_2H_4 is dramatically changed by wall

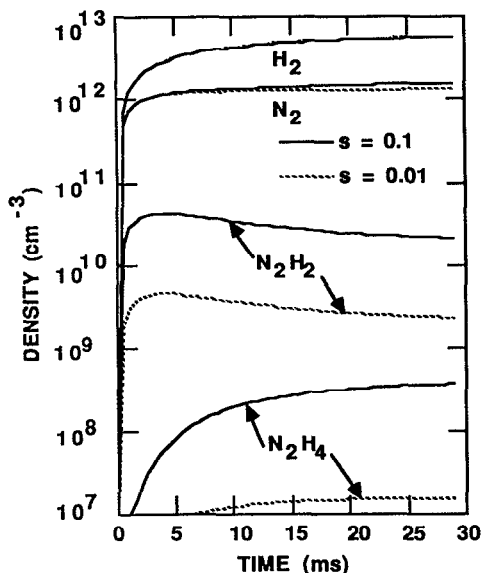
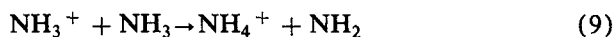


FIG. 2. Results of a computer experiment investigating the influence of wall reactions in ammonia chemistry. A $\text{NH}_3/\text{NH}_2/\text{H} = 99.8/0.1/0.2$ gas mixture was flowed through a cylindrical vessel (radius 4 cm) with wall reactions as given by Eq. (8). The probability of association reactions on the wall is either $s = 0.01$ or 0.1 . The production of N_2H_2 and N_2H_4 is most sensitive to wall reactions. The production of N_2 and H_2 is least sensitive.

reactions. The production of NNH decreases when including wall reactions due to the more rapid loss of H .

The electron-impact ionization of NH_3 has major branchings to NH_3^+ and NH_2^+ , with appearance potentials of 10.2 and 16.6 eV, respectively.^{42,64} The lower threshold for NH_3^+ results in its rate of production being larger. In either case, conversion to NH_4^+ is rapid (see below). Hayashi²¹ identifies two electronic states for electron-impact excitation of NH_3 with threshold energies of 5.6 and 8.9 eV. Photolysis of NH_3 for wavelengths of $217 \text{ nm} > \lambda > 166 \text{ nm}$ produces $\text{NH}_2 + \text{H}$.⁴² The 5.6 eV process cited by Hayashi most likely corresponds to exciting this state, and we assigned the same dissociative branching. The 8.9 eV electronic excitation process was assigned a branching to $\text{NH} + 2\text{H}$.

Charge-exchange reactions of ammonia ions in ammonia are rapid and most likely result in abstracting H leading to formation of NH_4^+ . For example,



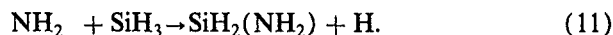
has a rate coefficient of $2.2 \times 10^{-9} \text{ cm}^3 \text{ s}^{-1}$.⁴³ Given its exothermicity one can, by analogy, expect that reaction of NH_2^+ with ammonia will also be rapid and result in a H abstraction,



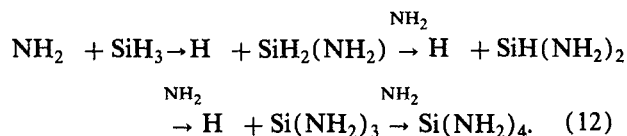
We estimated the rate coefficient for this process to be $1 \times 10^{-9} \text{ cm}^3 \text{ s}^{-1}$.

E. Plasma kinetics: $\text{SiH}_4\text{-NH}_3$

The reactions describing silane-ammonia plasma chemistry used in the model are also listed in Table III. Beach and Jasinski recently investigated the neutral kinetics of ammonia-silane mixtures.²⁹ They found that amino radicals, nearly unreactive with SiH_4 , readily insert into SiH_3 and eliminate hydrogen forming amino-silane complexes. For example,



Successive insertions of NH_2 into the complex continues to add amino groups and eliminate H , until reaching $\text{Si}(\text{NH}_2)_4$:



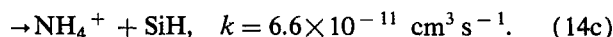
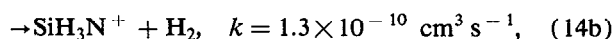
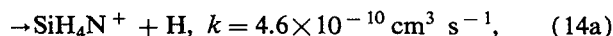
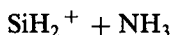
With the exception of the final product, the intermediate complexes $\text{Si}_{3-n}(\text{NH}_2)_n$ retain a dangling bond, thereby helping to explain their reactivity. Free H atoms saturate the $\text{Si}_{3-n}(\text{NH}_2)_n$ complexes, forming $\text{Si}_{4-n}(\text{NH}_2)_n$. H atoms, however, readily abstract H from silane, and in analogy to those reactions we estimated that H also abstracts hydrogen from the saturated amino-silane complexes. For example,



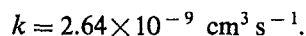
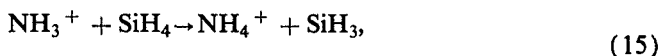
has an estimated exothermicity of 12 kcal/mol and we assigned rate coefficients of $5 \times 10^{-11} \text{ cm}^3 \text{ s}^{-1}$ for these processes.

The products of reactions of NH with SiH_4 have not been measured. Insertion reactions of NH into SiH_4 producing amino-silane complexes should be exothermic. When energetically permitted, we estimated that reactions of NH_n ($n = 1, 2$) with SiH_n ($n \leq 4$) form amino-silane complexes with rate coefficients of $1\text{--}5 \times 10^{-11} \text{ cm}^3 \text{ s}^{-1}$.

The ion chemistry of SiH_4/NH_3 mixtures was recently studied by Haller,⁴⁴ whose results are included in Table III. Reactions of silane ions with ammonia most likely cluster, and least likely proton exchange. For example, the most likely reactions for SiH_2^+ with NH_3 are

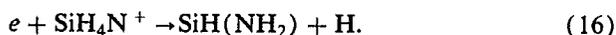


Similarly, reactions of SiH_nN^+ ions with silane and ammonia are also likely to cluster. Ammonia ions, though, will most likely abstract hydrogen from silane, either as part of a charge-exchange reaction or independent of a charge exchange. For example, the most likely branchings for reactions of ammonia ions with silane are



The tendency for ions in SiH₄/NH₃ mixtures is then to either protonate, or to form SiH_nN⁺ clusters. NH₄⁺ and Si₂H₆N⁺ are terminal species.

The products of the dissociative recombination of NH₄⁺ are believed to be primarily NH₃ + H.⁴² In analogy to this finding, we estimated that dissociative recombination of NH_n⁺ (*n* = 2,3) also branches to NH_{n-1}⁺ + H. The products of the dissociative recombination of SiH_nN⁺ ions are not known. Breaking the Si—N bond is energetically costly, and so elimination of H was chosen as the dissociation product. For example,

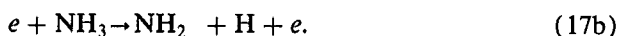
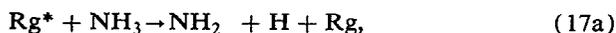


The rate coefficients of all dissociative recombinations of NH_n⁺ and SiH_nN⁺ were estimated to be $1.1 \times 10^{-7}/T_e^{1/2} \text{ cm}^3 \text{ s}^{-1}$, where *T_e* is the electron temperature (eV). This rate is analogous to that for methane ions.⁴⁵

F. Deposition precursors and surface kinetics

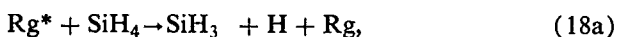
The deposition of Si₃N₄ by DPECVD and RPACVD typically uses gas mixtures containing rare gases, NH₃, SiH₄, and N₂. There are two interesting regimes for deposition which we call “molecular” and “atomic.” In the molecular regime, the gas mixtures typically contain NH₃ and SiH₄. The precursors to the deposition are believed to be the amino-silane complexes described above. Smith *et al.*⁴⁶ found that SiH_{4-n}(NH₂)_n and disilane were the most plentiful products in DPECVD using SiH₄/NH₃ mixtures.

The precursors to the amino-silane complexes in RPACVD, NH₂, and SiH₃ are likely to be produced by different mechanisms. NH₂ radicals are dominantly produced by excitation transfer and electron impact,



Since H is unreactive with NH₃ at moderate gas temperatures (< hundreds of °C) production of NH₂ by H abstraction from NH₃ is not significant. NH₂ is also surprisingly unreactive with SiH₄. The rate coefficient for the abstraction of H from SiH₄ by NH₂ is $8 \times 10^{-14} \text{ cm}^3 \text{ s}^{-1}$.^{29,47} In low-temperature systems, this reaction path can be almost ignored and does not deplete NH₂.

Downstream of the plasma zone SiH₃ radicals are produced dominantly by excitation transfer and abstraction reactions,



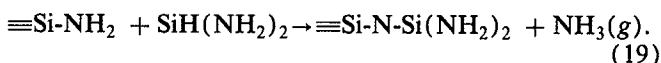
The source of H in the abstraction reaction is either the previous excitation transfer step or reactions that generate NH₂. In this regard, generating a single NH₂ radical will, with high probability, ultimately produce both reactants required for producing an amino-silane complex provided that diffusion and other reactions do not deplete the radicals. Additional reactions of NH₂ with SiH_n(NH₂)_{4-n} liberate H which can produce additional SiH₃ by H abstrac-

tions. The rate-limiting step in producing the deposition precursor is therefore generating sufficient densities of NH₂.

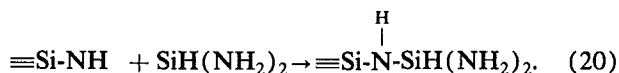
The gas mixtures in the “atomic” deposition regime are, for example, N₂/SiH₄. In DPECVD, N₂/SiH₄ mixtures were found to generate virtually no Si-N precursors in the plasma.⁴⁸ This may result from the unreactive nature of the fragments. The abstraction of H from SiH₄ by N is endothermic by approximately 11.4 kcal/mol. The insertion of N into a Si—H bond, forming SiH₂(NH₂) is exothermic with either the elimination of H₂ or 2H. The transition state corresponding to NH-SiH₃, however, is estimated to be endothermic. Therefore, SiH₄/N₂ plasmas that do not have a significant amount of dissociation of SiH₄ and N₂ leading to radical-radical reactions have little interesting chemistry. For example, the abstractions of H from both SiH₃ and SiH₂ by N are exothermic by 6.6 and 4.4 kcal/mol, respectively. The abstractions of H from SiH₄ and SiH₃ by NH are also exothermic. The insertion of NH into SiH₄ eliminating H is also exothermic, with the transition state also being slightly exothermic. The lack of Si—N bonding in the gas phase observed by Smith and co-workers⁴⁸ for N₂/SiH₄ mixtures may imply that the insertion of N and NH into SiH₄ is not highly probable or that significant densities of NH₂ and SiH₃ were not simultaneously produced. In this respect, our estimate for the rate coefficient for NH insertion into SiH₄ was made less than gas kinetic.

Deposition in the atomic regime most likely results from a flux of radicals composed primarily of N, NH, and SiH₃. Films similar to those obtained in the atomic regime have been obtained using PECVD in which the feedstock gases are highly diluted by He.⁴⁹ The high dilution reduces the probability of radical-radical reactions, thereby ensuring that the deposition flux is composed mostly of monomers.

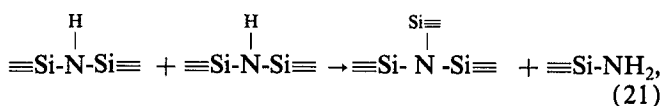
The surface deposition kinetics involving SiH_n(NH₂)_m precursors is not certain. A surface passivated by NH₂ can incorporate adsorbed SiH(NH₂)₂ by elimination of ammonia,⁴⁷



An adsorbed SiH(NH₂)₂ incorporating into a ≡Si-NH configuration, however, most likely retains a N—H bond,



Elimination of the NH bond is problematic due to the endothermicity of interconnection reaction between adjacent ≡N-H sites,



or adjacent ≡Si-H and ≡N-H sites,

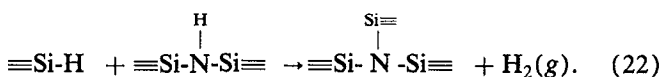


TABLE IV. Select surface reactions used in the model.

Species to surface	Branching for products (film or gas phase)			
Si	Film 0.9,	Si	0.1	
SiH	Film 0.8,	H ₂	0.4,	SiH 0.2
SiH ₂	Film 0.8,	H ₂	0.8,	SiH ₂ 0.2
SiH ₃	Film 0.1,	Si ₂ H ₆	0.05	
Si ₂ H _n , n < 4	Film 0.8,	H ₂	n · 0.4,	Si ₂ H _n 0.2
Si ₂ H ₅	Film 0.2,	H ₂	0.5	Si ₂ H ₅ 0.8
Si _n H _m ⁺		Si _n H _m	1.0	
NH		N ₂ H ₂	0.05,	NH 0.9
NH ₂		N ₂ H ₄	0.02,	NH ₂ 0.96
SiH _n (NH ₂) _{3-n}	Film 0.01–0.1,	SiH _n (NH ₂) _{3-n}	balance	
NH _n ⁺ , n < 3		NH _n	1.0	
NH ₄ ⁺		NH ₃	1.0,	H 1.0

In multipole SiH₄/NH₃ plasmas it was found that ≡Si—H bonding decreases and ≡N—H bonding increases as the SiH₄/NH₃ ratio decreased.⁵⁰ The increase in the NH₃ fraction suggests that there will be more ≡N—H bonding on the surface, and therefore suggests that interconnection between ≡N—H bonds is not particularly fast.

The boundary conditions for radicals and ions on the walls used in the model must include some estimate of sticking coefficients and surface reaction chemistries. Although many direct and indirect measurements for the reactive sticking coefficient of SiH₃ have been made,⁶⁵ there is little information available on the reaction of other species on cold walls, and so many of these reactions were estimated. The surface reactions used in the model are listed in Table IV.

III. SIMULATIONS OF RPACVD KINETICS

The geometry used in this study is intended to emulate that used in experiments of Lucovsky *et al.*⁸ as shown in Fig. 1. The reactor in our model is cylindrical with a diameter of 10 cm. The plasma is sustained in a narrower tube in the upstream portion of the reactor. Gases are initially flowed through the plasma zone and advect downstream to the mixing chamber. The secondary gases are injected from one or more circular rings in the mixing chamber. Unless otherwise noted, the gas pressure is 150 mTorr, the gas temperature is 350 K, and the flow rate is 400 sccm. This results in an average residence time in the reactor of approximately 0.05 s. The power deposition is approximately 0.1 W cm⁻³ and is restricted to the plasma zone, which is 3–5 cm in diameter. Gases enter from the left-hand side and are pumped out from the right-hand side. The circular injection nozzles are denoted by the black squares in the downstream reaction chamber. A circular stage that can hold a small substrate is coaxially mounted beginning at 22 cm. The contour plots shown below are two-dimensional slices through a reactor having azimuthal symmetry. In most figures, separate species are shown in the upper and lower halves of the diagrams. The contours are labeled with a fraction of the maximum density. The maximum value is noted adjacent to the figures. The contours may use either log or linear scales; the distinction is clear from the labels. Some contours have been

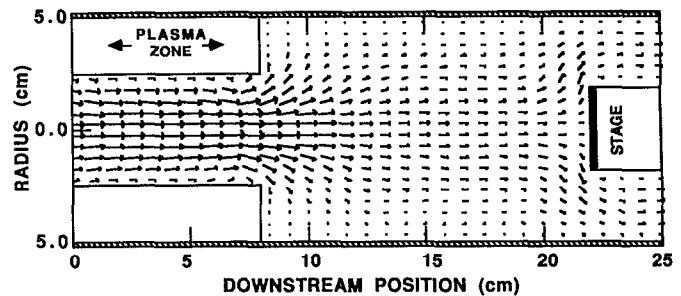


FIG. 3. Advective flow field for typical reactor conditions (Ar, 150 mTorr, 350 K, 400 sccm). The radial velocities have been exaggerated by a factor of 5 for presentation purposes.

selectively removed from the figures for clarity. The advective flow field for typical conditions is shown in Fig. 3.

A. Pure rare gases

The ion and metastable densities for pure Ar and He flowing through the plasma zone are shown in Fig. 4. The metastable densities are $\approx 10^{12}$ cm⁻³ while the ion densities are $5-10 \times 10^{10}$ cm⁻³. The dominant losses for the excited states are electron collisions causing superelastic relaxation or ionization, diffusion to the walls, and mutual quenching resulting from Penning reactions. As the plasma leaves the upstream chamber the electrons quickly cool. This reduces the source for the excited states by electron-impact excitation of ground-state atoms. The electrons can, however, continue to collisionally relax the excited states. The densities of the metastable atoms therefore quickly begin to decay. The rate coefficient for mutual quenching,

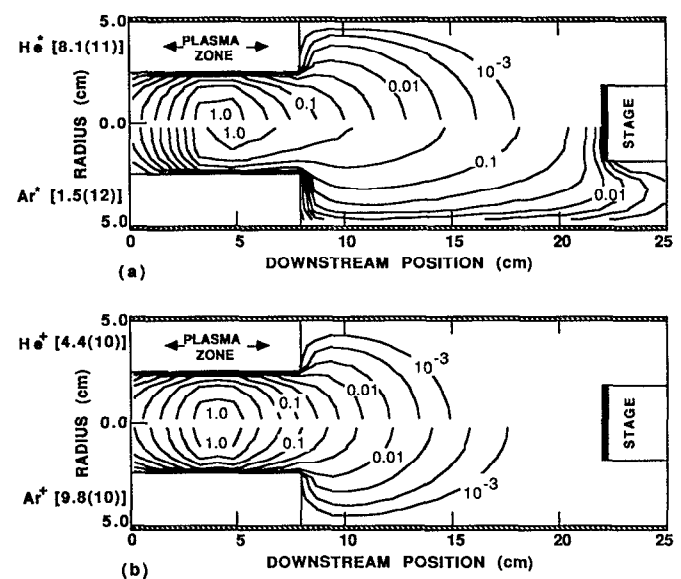


FIG. 4. Species densities for pure rare gases (Ar and He) in a RPACVD reactor: (a) metastable densities and (b) ion densities. The maximum densities (cm⁻³) are noted for each species and contour labels show the fraction of the maximum density. The gas pressure is 150 mTorr (350 K, 400 sccm). Excited-state densities generally penetrate further downstream than the ion densities.

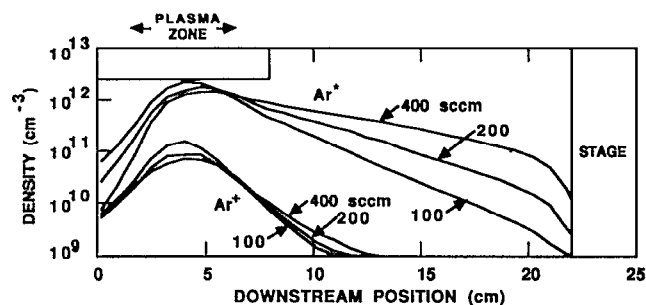


FIG. 5. Ar^* and Ar^+ densities along the axis of the RPACVD reactor for different flow rates (150 mTorr, 350 K). At high flow rates, the Ar^* penetrates far downstream.

or energy pooling, by the metastables are 1.5×10^{-9} and $5 \times 10^{-12} \text{ cm}^3 \text{ s}^{-1}$ for He^* and Ar^* . The higher rate of quenching of He^* and for the loss by diffusion results in a more rapid decrease in the helium metastables compared to the argon metastables. The Ar^* therefore penetrates further downstream and may reach the substrate with high flow rates. The electron density is too low for recombination with atomic ions to be an important loss process. Therefore the dominant loss for ions is recombination at the walls which is somewhat enhanced by epithermal electrons. The penetration of Ar^+ and He^+ downstream is roughly the same and for practical purposes they do not survive in appreciable numbers to reach the substrate. This is a surprising result since the mobility of He^+ is higher than that for Ar^+ and therefore one would expect more downstream penetration. The higher mobility of He^+ , though, also means that the rate of loss to the side walls is also greater. The transport of excited species into the mixing chamber for these conditions is roughly half diffusion and half advection. Experimental measurements of significant ion flux to the substrate can only be accounted for by generation of those ions locally, as opposed to transport from the upstream plasma zone. This may occur in systems with poorly confined capacitive coupling.

The degree to which the flow rate influences the penetration of excited states downstream is shown in Fig. 5 where the Ar^+ and Ar^* density is shown for flow rates of 100, 200, and 400 sccm. The rate of diffusion of the argon ions is ambipolar enhanced close to the plasma zone, and their penetration into the mixing chamber is a weak function of flow rate. The amount of penetration of Ar^* into the mixing chamber is largely determined by the flow rate. At flow rates of < 200 sccm, the transport is largely diffusion dominated.

B. R/SiH_4 chemistries

The deposition of α -Si:H and μc -Si is usually performed by flowing a rare gas through the plasma zone and injecting SiH_4 downstream. In the following cases, we have injected SiH_4 through a circular nozzle 5 cm in diameter located 4.5 cm from the narrow portion of the tube. The activation gases are either Ar or He. The total flow rate of

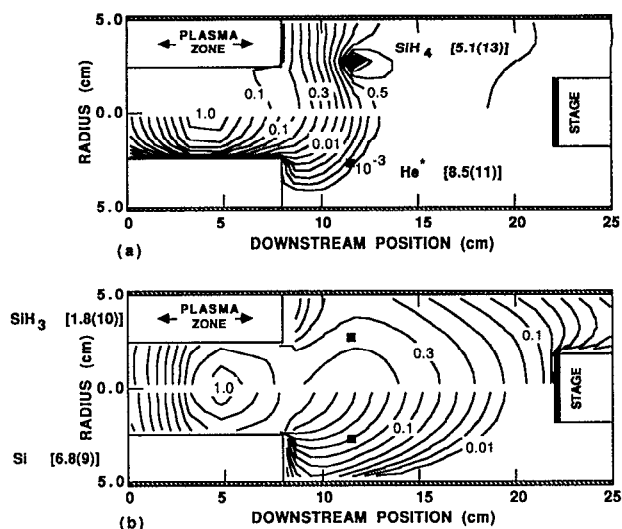


FIG. 6. Species densities for RPACVD using $\text{He}/\text{SiH}_4 = 99.5/0.5$ chemistry: (a) SiH_4 and He^+ and (b) SiH_3 and Si. The maximum densities (cm^{-3}) are shown adjacent to each species label. He is flowed through the reactor from the left-hand side and SiH_4 is injected through circular nozzles (denoted by black squares). The He^* does not penetrate far downstream as it is depleted by Penning reactions with backdiffusing SiH_4 . SiH_3 is produced both in the plasma zone and downstream in the mixing chamber.

SiH_4 through the nozzle is 0.05 that of the Rg flowing through the plasma zone.

Using the He/SiH_4 chemistry computed densities of He^* , SiH_4 , SiH_3 , and Si are shown in Fig. 6. The SiH_3 and Si radicals were selected as being examples of radicals that are desirable (SiH_3) and undesirable (Si) for depositing device quality films in DPECVD. In spite of the high flow rate (400 sccm) the injected silane diffuses upstream and penetrates into the plasma zone. Downstream of the nozzle, however, the SiH_4 density is fairly uniform. The helium metastable atoms encounter the backdiffusing silane as they emerge from the plasma zone. The silane quickly quenches and depletes He^* by Penning ionization reactions, thereby preventing its penetration very far into the mixing chamber.

The SiH_3 density has two maxima. The first is in the plasma zone and the second is downstream in the mixing chamber. The maximum in the plasma zone results from the backdiffusion of silane. In the plasma zone, silane is dissociated both directly by electron impact and by excitation transfer from He^* and He^+ . The secondary maxima downstream result dominantly from H abstraction from SiH_4 ($\text{H} + \text{SiH}_4 \rightarrow \text{SiH}_3 + \text{H}_2$). The H atoms are primarily produced in the plasma zone and convect downstream, or are produced by Penning reactions of SiH_4 with He^* . The SiH_3 flux at the substrate is approximately 10% of its maximum value in the plasma zone. SiH_3 that does not stick to the substrate or walls is quickly swept past the stage as the advective velocity increases in the narrowed portion of the chamber.

The Si atom density is maximum in the plasma zone, a consequence of direct electron-impact dissociation of si-

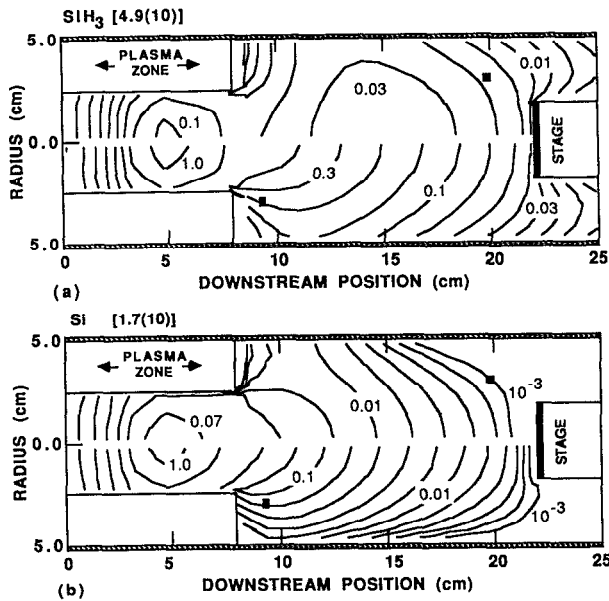


FIG. 7. Densities of (a) SiH_3 and (b) Si when placing the injection nozzles for SiH_4 adjacent to (bottom half of figure) and far from (top) the plasma zone. The maximum species densities (cm^{-3}) are shown adjacent to each species label. Conditions are otherwise the same as for Fig. 8. Moving the injection nozzle downstream increases the ratio of SiH_3/Si which flows to the substrate.

lane. In spite of a moderate production of Si in the plasma zone, it is fairly reactive with SiH_4 and has a high sticking coefficient on the walls. The Si flux, therefore, does not survive to reach the substrate in large quantities. These conditions are not particularly conducive to producing select radical fluxes by chemical isolation due to the backdiffusion of SiH_4 into the plasma zone. These conditions are, though, exemplary of obtaining a selective flux to the surface by physical isolation.

The typical growth rates of films grown by RPACVD are 1–10 $\text{\AA}/\text{min}$ with the lower rate being typical of epitaxial growth and the higher value typical of amorphous growth.⁸ The radical density incident onto the substrate can be related to the deposition rate by

$$N_s (\text{cm}^{-3}) \approx 2 \times 10^8 [r_D (\text{\AA}/\text{min})] / s,$$

where s is the reactive sticking coefficient. Deposition rates of 1–10 $\text{\AA}/\text{min}$ for radicals having sticking coefficients of 0.15 requires downstream radical densities of 1×10^9 – $1 \times 10^{10} \text{ cm}^{-3}$. These radical densities are commensurate with those predicted here.

The placement of the nozzles delivering the SiH_4 in part determines the selectivity of producing radicals. The densities of SiH_3 and Si for the He/SiH_4 chemistry are shown in Fig. 7 for nozzles that are 1 and 12 cm into the mixing chamber (approximately 3 and 14 cm from the plasma zone). The location of the maximum production of these radicals is in the plasma zone due to backdiffusion of SiH_4 , but is reduced by a factor of 10 by placing the nozzles downstream. The production of both SiH_3 and Si are larger downstream when placing the nozzles further from the

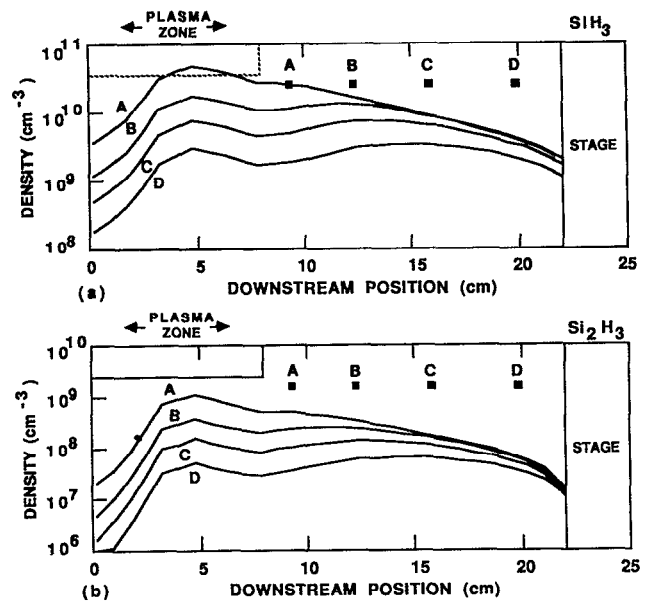


FIG. 8. Densities of (a) SiH_3 and (b) Si_2H_3 along the axis of the RPACVD reactor for four SiH_4 nozzle locations (labeled A–D). The chemistry is $\text{He}/\text{SiH}_4 = 0.95/0.05$ (150 mTorr, 350 K, 400 sccm). For conditions where silane leaks into the plasma zone, only large displacements of the injection nozzles significantly change the fluxes of radicals to the substrate.

plasma zone because the penetrations of He^* and He^+ into the mixing chamber are greater. The relative downstream production of SiH_3 is, however, greater than the Si . The end result is that the SiH_3/Si ratio incident on the substrate is greater when placing the nozzles downstream. In doing so, the chemical component of isolation is increased.

The densities of SiH_3 and Si_2H_3 on the axis of the chamber, examples of desirable and undesirable radicals for deposition, are shown for four different nozzle placements in Fig. 8. The conditions are otherwise the same as for Fig. 7. These results are shown here to demonstrate that wide variations in the placement of the nozzles do not necessarily directly correlate with dramatic changes of fluxes to the surface. These results can also be explained by leakage of silane into the plasma zone, which nonselectively produces radicals by electron impact. In this respect, other methods must be used to improve the isolation of SiH_4 from the plasma zone.

If the flow rate and geometry are not changed, poor physical isolation of the injected silane from the plasma zone is not significantly improved by changing the gas pressure. Decreasing the gas pressure increases the advective velocity. However, the rate of backdiffusion of silane to the plasma zone also increases by the same proportion. Either the flow rate or geometry must be changed to affect the isolation characteristics. In the following examples, we have narrowed the plasma zone to a diameter of 3 cm while keeping the flow rate constant, thereby increasing the advective velocity through the plasma zone and into the reaction chamber. The injected silane will be better isolated

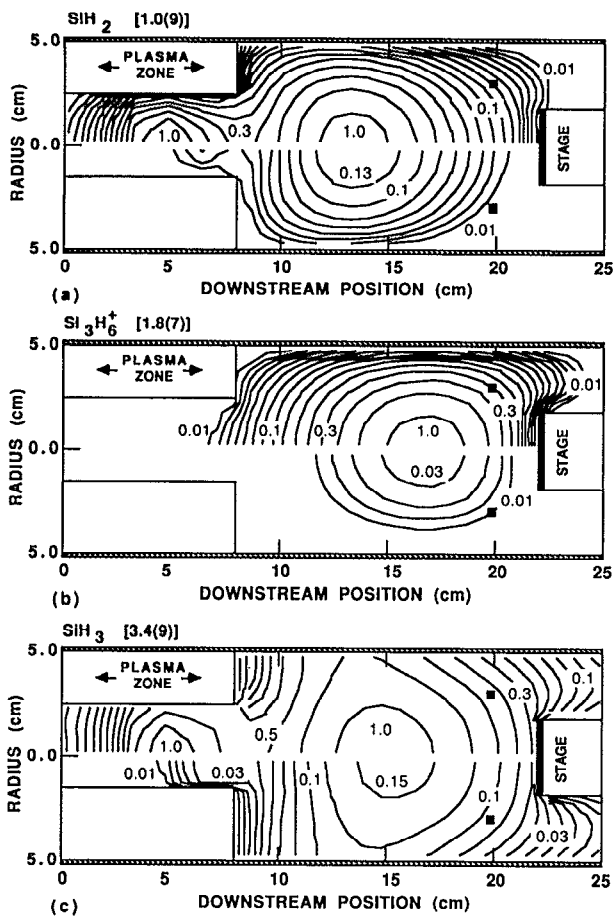


FIG. 9. Radical and ion densities [maximum values (cm^{-3}) shown adjacent to each species label] for two different diameters of the plasma zone (3 and 5 cm): (a) SiH_2 ; (b) Si_3H_6^+ ; and (c) SiH_3 . Densities for the smaller diameter plasma zone are shown in the lower half of each figure. The chemistry is He/ SiH_4 (150 mTorr, 350 K, 400 sccm). He flows through the plasma zone while SiH_4 is injected downstream through nozzles shown by black squares. The higher velocity and smaller opening to the plasma zone combine to reduce the leakage of SiH_4 into the plasma zone and lower the flux of SiH_2 and Si_3H_6^+ to the substrate.

from the plasma zone because backdiffusion is less able to overcome the higher advective velocity, and the opening to the plasma zone is physically smaller.

The densities of SiH_2 , Si_3H_6^+ , and SiH_3 using He/ SiH_4 chemistry for wide and narrow plasma zones are shown in Fig. 9. The silane nozzles are placed approximately at 20 cm, or 12 cm from the narrow portion of the chamber. SiH_2 is generally considered undesirable for high-quality deposition while SiH_3 is generally considered the desirable deposition radical. The density of the trimer ion is an indication of the importance of higher-order ion chemistry. Although the contribution of higher-order ions to film growth is not known, it is generally accepted that they are not desirable for high-quality films. The production of SiH_2 and SiH_3 is reduced by a factor of 8, and that of Si_3H_6^+ by a factor of 30 by using the narrower nozzle thereby isolating silane from the plasma zone. However, due to the higher reactivity of SiH_2 and Si_3H_6^+ their fluxes to the substrate are reduced to even a greater degree than

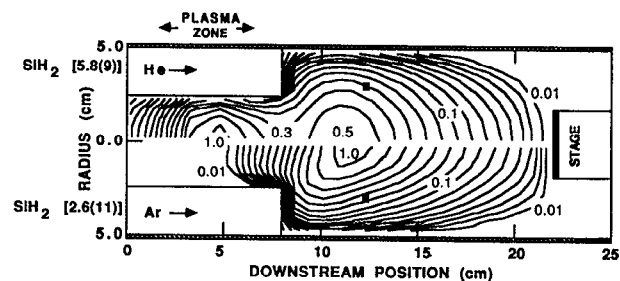


FIG. 10. A comparison of SiH_2 densities [maximum values (cm^{-3}) shown in each case] for RPACVD using He/ SiH_4 chemistry (top half of figure) and Ar/ SiH_4 chemistry (bottom half of figure). Due to the leakage of SiH_4 into the wide plasma zone, substantial amounts of SiH_2 are produced using the He/ SiH_4 chemistry.

SiH_3 . The end result is a more selective flux of radicals to the substrate which favors SiH_3 .

To capitalize on the selective fragmentation patterns of injected deposition gases by excitation transfer from the activated gases, the injected gases must be isolated from the plasma zone. Evidence for the selectivity of these processes

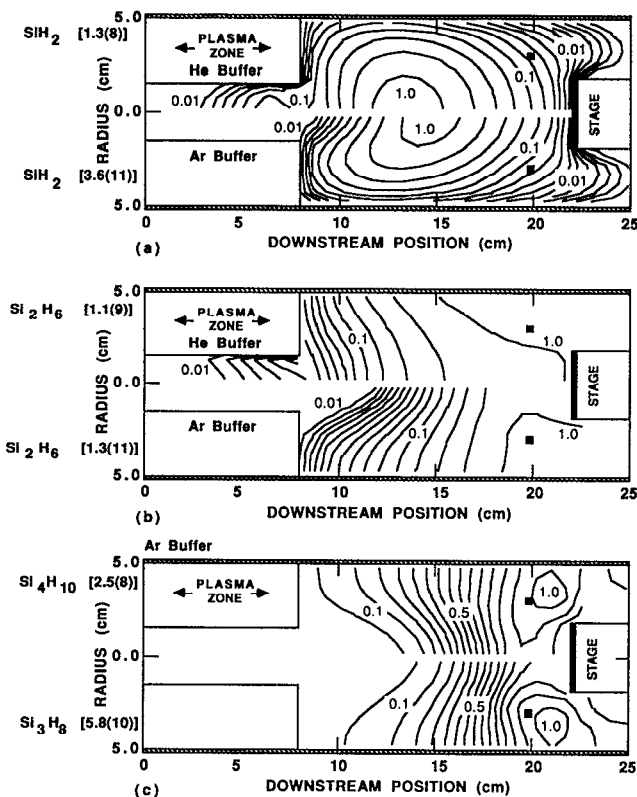
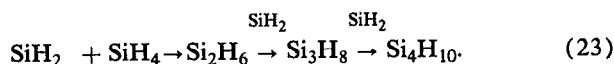


FIG. 11. Species densities in the silane polymerization chain based on SiH_2 insertion using Ar/ SiH_4 and He/ SiH_4 chemistries. The narrow plasma zone isolates SiH_4 from the plasma. The mixtures are $\text{Rg}/\text{SiH}_4 = 95/5$ with SiH_4 being injected from the nozzles downstream (black squares). The maximum densities (cm^{-3}) are shown adjacent to each species label: (a) SiH_2 for He/ SiH_4 (top) and Ar/ SiH_4 (bottom); (b) Si_2H_6 for He/ SiH_4 (top) and Ar/ SiH_4 (bottom); (c) Si_3H_8 and Si_4H_{10} for the Ar/ SiH_4 chemistry. The selective fragmentation of SiH_4 by Rg^* and Rg^+ leads to higher-order silanes in the Ar/ SiH_4 system which are absent in the He/ SiH_4 system.

was discussed by Lucovsky and co-workers.¹⁰ RPACVD of α -Si:H using He/SiH₄ chemistries resulted in high-quality depositions, whereas RPACVD using Ar/SiH₄ chemistries resulted in gas-phase polymerization and poor quality films. A reactor configuration for RPACVD that results in nonselective dissociation of SiH₄ is shown in Fig. 10 for Ar/SiH₄ and He/SiH₄ chemistries. Here the density of SiH₂ is plotted, a precursor to gas-phase polymerization (see discussion below). Substantial amounts of SiH₂ are produced in each case. The wide opening to the plasma zone and close proximity of the nozzles allows backdiffusion of SiH₄ into the plasma zone which results in nonselective dissociation of SiH₄ for He/SiH₄ mixtures. SiH₂ is produced by electron impact and is also a direct product of quenching by Ar* in the Ar/SiH₄ chemistry in any case.

Selective RPACVD is shown in Fig. 11 where the densities of SiH₂, Si₂H₆, Si₃H₈, and Si₄H₁₀ appear for Ar/SiH₄ and He/SiH₄ chemistries. The species are members of the polymerization chain based on silylene insertion,



Selective fragmentation of SiH₄ is achieved by using a narrow plasma zone and placing the SiH₄ nozzles far downstream. These conditions prevent significant dissociation of SiH₄ in the plasma zone, thereby relying on the excitation transfer reactions from Rg* and Rg⁺ for fragmentation. The density of SiH₂ is reduced by a factor of 10³ using the He/SiH₄ chemistry relative to the Ar/SiH₄ chemistry. Due to the higher rate of diffusion of SiH₄ in He compared to Ar, there is more leakage of silane into the plasma zone using the He/SiH₄ chemistry, but this does not substantially increase the production of SiH₂. In both cases, the production of SiH₂ is maximum downstream where the plumes of Rg* and Rg⁺ meet the backdiffusing silane. The production of Si₂H₆ in the He/SiH₄ case is similarly reduced by a factor of 10². In the He/SiH₄ chemistry, Si₃H₈ and Si₄H₁₀ have negligibly small densities, and so their values are not shown. The densities of Si₃H₈ and Si₄H₁₀ for the Ar/SiH₄ chemistry are shown in Fig. 11(c). Their densities increase with distance from the plasma zone as the SiH₂ radicals have more opportunity to proceed up the polymerization chain. Since the saturated silane species have low sticking coefficients, the Si₃H₈ and Si₄H₁₀ are eventually swept by the stage and exit the mixing chamber.

C. Rg/NH₃/SiH₄ chemistries

The RPACVD of Si₃N₄ is typically performed by passing Rg, Rg/N₂, or Rg/NH₃ through the plasma zone, and injecting SiH₄ (and NH₃) downstream. It has been suggested that amino-silane complexes such as SiH₂(NH₂), which are initially formed by reactions between SiH₃ and NH₂, are the deposition precursors. Higher-order amino-silane complexes are formed by successive reactions with amino radicals.

Our first demonstration system uses He/NH₃/SiH₄ chemistry. He/NH₃ is flowed through the plasma zone and SiH₄ is injected downstream. A narrow plasma zone with

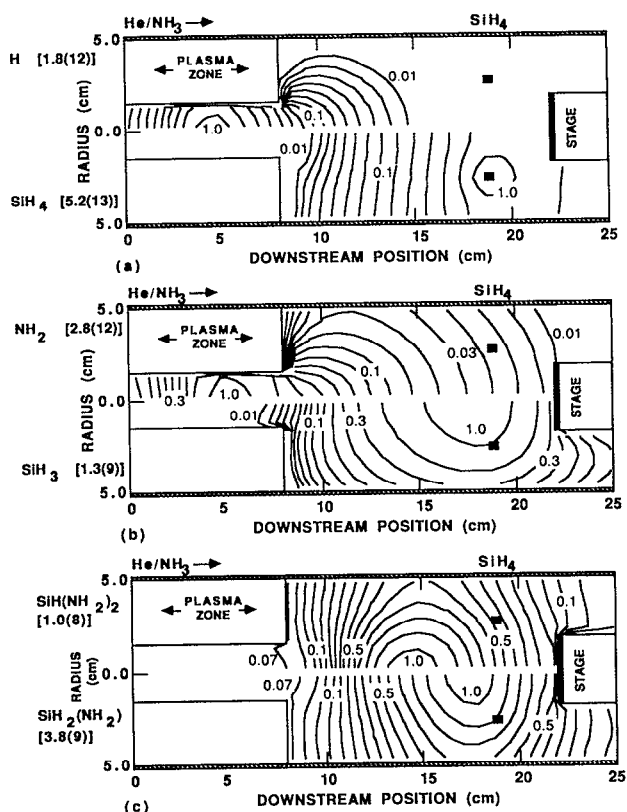


FIG. 12. Species densities in Si₃N₄ RPACVD using He/NH₃/SiH₄ = 0.85/0.1/0.05 (150 mTorr, 350 K, 400 sccm). He/NH₃ is flowed through the plasma zone and SiH₄ is injected through the nozzles downstream. The maximum species densities (cm⁻³) are shown adjacent to the species labels: (a) H (top) and SiH₄ (bottom); (b) NH₂ (top) and SiH₃ (bottom); (c) SiH(NH₂)₂ (top) and SiH₂(NH₂) (bottom). The majority of SiH₃ is produced by H abstraction by H from SiH₄. NH₂ is produced in the plasma zone and reacts with SiH₃ to form the deposition precursor SiH₂(NH₂).

the SiH₄ nozzles placed downstream are used to maximize the isolation of SiH₄ from the plasma zone. The input gases have the ratios He/NH₃/SiH₄ = 0.85/0.1/0.05. Densities for H, SiH₄, NH₂, SiH₃, SiH₂(NH₂), and SiH(NH₂)₂ are shown in Fig. 12 for these conditions. The densities of He* and He⁺ (not shown) are greatly diminished compared to the case where only the Rg is flowed through the plasma zone. The very rapid Penning and charge-exchange reactions of He* and He⁺ with NH₃ deplete their densities. As a result, He* and He⁺ are strictly confined to the plasma zone.

Since He* and He⁺ are confined to the plasma zone and SiH₄ is nearly isolated from the plasma zone [see Fig. 12(a)], silane is not appreciably dissociated by excitation transfer reactions as it is in the He/SiH₄ system. Here the majority of fragmentation of SiH₄ results from H abstraction (H + SiH₄ → SiH₃ + H₂). Atomic hydrogen [shown in Fig. 12(a)] is produced by dissociation of NH₃ in the plasma zone, and convects into the mixing chamber. At the intersection of the backdiffusing SiH₄ and the H, SiH₃ is produced by hydrogen abstraction, as shown in Fig. 12(b). NH₃ is dissociated roughly equally by excitation transfer

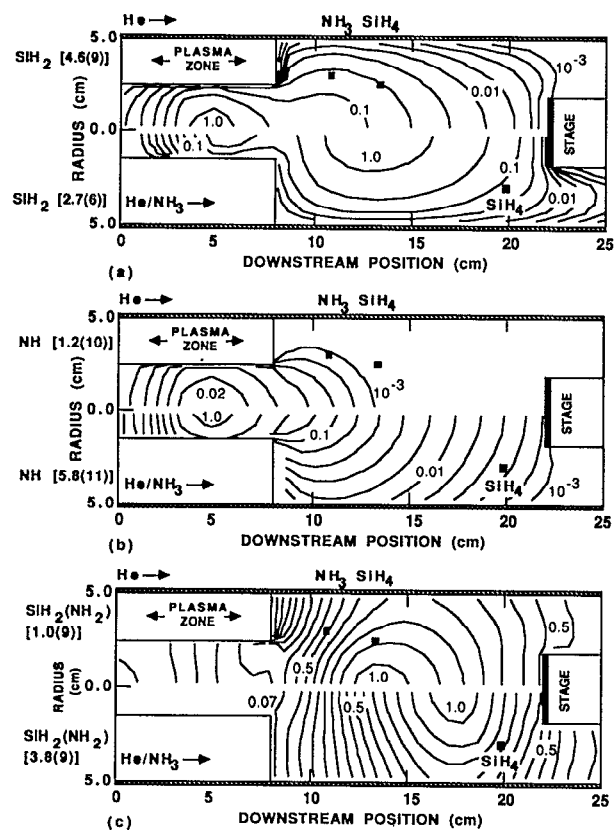


FIG. 13. Comparison of He/NH₃/SiH₄ chemistries for RPACVD of Si₃N₄ when He/NH₃ is flowed through a narrow plasma zone (configuration I in the lower half of the figures) and when only He is flowed through a wide plasma zone (configuration II in the top half of the figures). The remaining gases are injected through nozzles as shown: (a) SiH₂; (b) NH; and (c) SiH₂(NH₂). The maximum species densities (cm⁻³) are shown adjacent to the species labels. The final fluxes of SiH₂(NH₂) to the substrate are similar in each case. The fluxes of NH and SiH₂, though, are quite different.

from the excited Rg and direct electron-impact dissociation in the plasma zone. The major product is NH₂, which also convects out of the plasma zone as shown in Fig. 12(b). The amount of production of NH₂ in the mixing chamber is negligibly small due to the inability for H or SiH₃ to abstract H from NH₃. The first deposition precursor, SiH₂(NH₂), is produced by reactions between NH₂ and SiH₃, with densities as shown in Fig. 12(c). The density of the next higher-order precursor, SiH(NH₂)₂, is also shown in Fig. 12(c). The densities of higher-order precursors decrease by roughly an order of magnitude for each additional step in the sequence. Based on this analysis, SiH₂(NH₂) and SiH(NH₂)₂ are the only important amino-silane complexes to contribute to the deposition.

The fluxes of the amino-silane complexes to the substrate imply a deposition rate of $\approx 1 \text{ \AA}/\text{min}$ for a reactive sticking coefficient (RSC) of 0.1, though they may have a lower values. The observed deposition rates may therefore be explained by the amino-silane complexes. However the fluxes of SiH₃ and NH₂ to the substrate are at least equal to or exceed that of the amino-silane complexes and likely

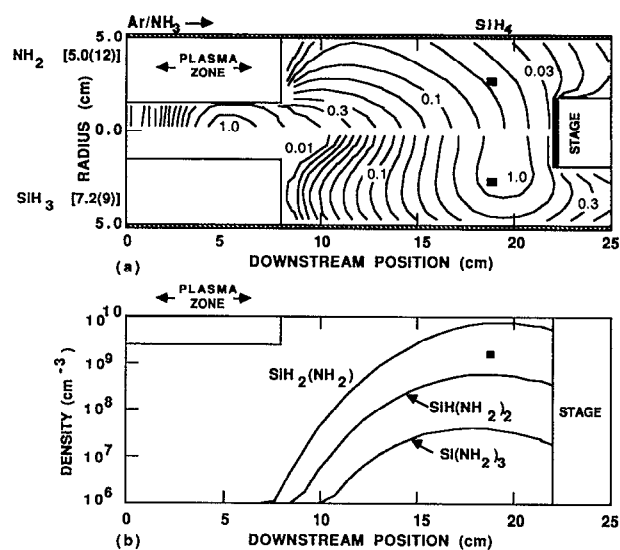


FIG. 14. Densities of (a) SiH₃ and NH₂ [maximum values (cm⁻³) shown by each species label] and (b) amino-silane complexes along the axis of the RPACVD reactor. The chemistry is Ar/NH₃/SiH₄ = 0.85/0.1/0.05 (150 mTorr, 350 K, 400 sccm). Ar/NH₃ is flowed through the plasma zone while SiH₄ is injected downstream. The production of the deposition precursors is somewhat larger than the He/NH₃/SiH₄ chemistry due to lower losses of NH₂ and SiH₃ to diffusion.

have a higher RSC. They could conceivably significantly contribute to the deposition.

The placement of nozzles and the choice of gases flowed through the plasma zone involve a series of trade-offs. As an example, we compared two reactor configurations using the He/NH₃/SiH₄ chemistry. In configuration I (bottom contours in Fig. 13), He/NH₃ is flowed through the plasma zone and SiH₄ is injected far downstream. In configuration II (top contours in Fig. 13), only He is flowed through the plasma zone. SiH₄ and NH₃ are injected through separate nozzles adjacent to the plasma zone. The plasma zone is also wider than configuration I, thereby compromising the isolation of the injected gases from the plasma zone. Densities of SiH₂, NH, and SiH₂(NH₂) in these two configurations are compared in Fig. 13. SiH₂ and NH are examples of "sticky" radicals which presumably do not produce high-quality films while SiH₂(NH₂) is the desired precursor. In configuration I, the production of SiH₂ is very low [as shown in the lower half of Fig. 13(a)]. It is produced in small quantities in the plasma zone and by H abstraction from SiH₃ downstream. Production of SiH₂ in configuration II [shown in the upper half of Fig. 13(a)] is 10³ times larger, as it is produced dominantly by penetration of SiH₄ into the plasma zone. The opposite behavior is observed for the production of NH, as shown in Fig. 13(b). In configuration I, the NH production is high since it is a direct product of electron-impact dissociation in the plasma zone through which He/NH₃ is flowed. In configuration II, the NH production is also dominated by electron-impact dissociation, but the amount generated is 50 times smaller, and little survives to

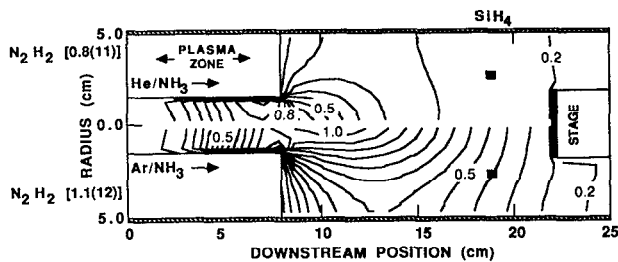


FIG. 15. N_2H_2 densities [maximum values (cm^{-3}) shown adjacent to the species label] for He/ NH_3 / SiH_4 (top) and Ar/ NH_3 / SiH_4 (bottom) chemistries. Rg/NH_3 is flowed through the plasma zone, and SiH_4 is injected downstream. Since the excited rare gases are confined to the plasma zone, the production of higher-order products is quite similar in each case.

reach the substrate. The final production of $SiH_2(NH_2)$ in these two configurations, as shown in Fig. 13(c), results in nearly the same flux of the deposition precursor to the plasma zone. In this respect, the choice of configuration I or configuration II for a particular application is predicated on differences in the production of secondary species, such as NH and SiH_2 , rather than the production of the direct deposition precursor.

The densities of SiH_3 and NH_2 and the axial densities of amino-silane complexes are shown in Fig. 14 for the Ar/ NH_3 / SiH_4 chemistry where Ar/ NH_3 is flowed through the plasma zone. The plasma zone is narrow to maximize isolation of the silane. As with the He/ NH_3 / SiH_4 chemistries, NH_2 is produced exclusively in the plasma zone and SiH_3 is produced in the mixing chamber dominantly by H abstraction. Due to the lower rate of diffusion of SiH_3 and NH_2 to the walls, their densities remain somewhat higher than using He chemistry. The result is that the production of amino-silane complexes is higher and shifted somewhat downstream.

RPACVD of Si_3N_4 using Ar/ NH_3 / SiH_4 and He/ NH_3 / SiH_4 in configuration I should yield quite similar results. The reason is that Rg^* and Rg^+ are both confined to the plasma zone and therefore differences in fragmentation of SiH_4 by excitation transfer are not important. The dissociation of NH_3 is roughly half by electron impact and half by excitation transfer from Rg^* and Rg^+ . The former process is not a sensitive function of the rare gas, while the latter processes yield similar fragments. Penning reactions by Rg^* and charge exchange from Rg^+ produce either NH_2^+ or NH_3^+ , both of which rapidly produce NH_4^+ by charge exchange with NH_3 . We compared Ar/ NH_3 / SiH_4 and He/ NH_3 / SiH_4 chemistries using configuration I and found that the production of deposition precursors and intermediates was quite similar. For example, the density of N_2H_2 produced using Ar and He chemistries in configuration I is shown in Fig. 15. Although there are subtle differences in the spatial distribution between the two chemistries, the amount of N_2H_2 produced and the flux of N_2H_2 to the substrate are nearly the same.

IV. CONCLUDING REMARKS

A model for RPACVD has been developed and the deposition of silicon alloys using $Rg/NH_3/SiH_4$ ($Rg = He, Ar$) mixtures has been investigated. We found that selective fragmentation of SiH_4 by excitation transfer from Rg^* and Rg^+ can be capitalized on to produce desirable fluxes to the substrate using He/ SiH_4 and Ar/ SiH_4 mixtures. Isolation of SiH_4 from the plasma zone, though, is an important issue. The analogous processes in $Rg/NH_3/SiH_4$ mixtures where Rg/NH_3 is flowed through the plasma zone are less important since excited states of the rare gases are rapidly quenched and restricted to the plasma zone. By carefully selecting flow rates and geometries one can control the flux of radicals to the substrate, though selectivity must often be traded off against a lower deposition rate.

ACKNOWLEDGMENTS

The author would like to thank G. Lucovsky, R. Markunas, and N. Masnari for their comments and advice. The author would also like to thank T. Sommerer for his reading of the manuscript, and M. E. Webber for comments on reaction chemistries. This work was supported by the Semiconductor Research Corporation, the National Science Foundation (Grants No. ECS91-09326 and CTS91-13215), and the University of Wisconsin Engineering Research Center for Plasma Aided Manufacturing.

- ¹D. L. Flamm and G. K. Herb, in *Plasma Etching: An Introduction*, edited by D. M. Manos and D. L. Flamm (Academic, San Diego, 1989), Chap. 1.
- ²R. C. Ross and J. Jaklik, Jr., *J. Appl. Phys.* **55**, 3785 (1984).
- ³R. Reif and W. Kern, in *Thin Film Processes II*, edited by J. L. Vossen and W. Kern (Academic, Boston, 1991), pp. 525-564.
- ⁴J. C. Knights and R. A. Lujan, *Appl. Phys. Lett.* **35**, 244 (1979).
- ⁵R. Field, D. F. Klemperer, P. W. May, and Y. P. Song, *J. Appl. Phys.* **70**, 82 (1991).
- ⁶B. Gorowitz, T. B. Gorczyca, and R. J. Saia, *Solid State Technol.* **16**, 197 (1985).
- ⁷L. E. Kline and M. J. Kushner, *Crit. Rev. Solid State Mater. Sci.* **16**, 1 (1989).
- ⁸G. Lucovsky, D. Tsu, R. Rudder, and R. Markunas, in *Thin Film Processes II*, edited by J. L. Vossen and W. Kern (Academic, Boston, 1991), pp. 565-620.
- ⁹G. N. Parsons, D. V. Tsu, and G. Lucovsky, *J. Vac. Sci. Technol. A* **6**, 1912 (1988).
- ¹⁰G. Lucovsky, D. V. Tsu, and G. N. Parsons, in *Deposition and Growth: Limits for Microelectronics*, edited by G. W. Rubloff (AIP, New York, 1988), p. 172.
- ¹¹G. Lucovsky and D. V. Tsu, *J. Cryst. Growth* **86**, 804 (1988).
- ¹²G. Lucovsky, P. D. Richard, D. V. Tsu, S. Y. Lin, and R. J. Markunas, *J. Vac. Sci. Technol. A* **4**, 681 (1986).
- ¹³G. Lucovsky and D. V. Tsu, *J. Non-Cryst. Solids* **97&98**, 265 (1987).
- ¹⁴T. Hsu, L. Breaux, B. Anthony, S. Banerjee, and A. Tash, *J. Electron. Mater.* **19**, 375 (1990).
- ¹⁵B. Anthony, T. Hsu, L. Breaux, R. Qian, S. Banerjee, and A. Tash, *J. Electron. Mater.* **19**, 1089 (1990).
- ¹⁶L. Breaux, B. Anthony, T. Hsu, S. Banerjee, and A. Tash, *Appl. Phys. Lett.* **55**, 1885 (1989).
- ¹⁷J. C. Knights, R. A. Lujan, M. P. Rosenblum, R. A. Street, and D. K. Biegelsen, *Appl. Phys. Lett.* **38**, 337 (1981).
- ¹⁸M. J. Kushner, *J. Appl. Phys.* **63**, 2532 (1988).
- ¹⁹M. J. Kushner, *J. Appl. Phys.* **54**, 4958 (1983).
- ²⁰M. J. Kushner, *IEEE Trans. Plasma Sci.* **PS-14**, 188 (1986).

- ²¹M. Hayashi, in *Swarm Studies and Inelastic Electron-Molecule Collisions*, edited by L. C. Pitchford, V. B. McKoy, A. Chutjian, and S. Trajmar (Springer, New York, 1987), pp. 167-190.
- ²²He electron-impact cross sections were obtained from: Momentum transfer, M. Hayashi, Nagoya Institute of Technology Report IPPJ-AM-19, 1981; ionization, D. Rapp and P. Englander-Golden, *J. Chem. Phys.* **43**, 1464 (1965); excitation, J. P. Boeuf and E. Marode, *J. Phys. D* **15**, 2169 (1982).
- ²³Ar electron-impact cross sections were obtained from: Momentum transfer, M. Hayashi, Nagoya Institute of Technology Report IPPJ-AM-19, 1981; ionization, D. Rapp and P. Englander-Golden, *J. Chem. Phys.* **43**, 1464 (1965); excitation, K. Tachibana, *Phys. Rev. A* **34**, 1007 (1986).
- ²⁴D. Hershey, *Transport Analysis* (Plenum/Rosetta, New York, 1973), Chap. 3.
- ²⁵M. E. Coltrin, R. J. Kee, and G. H. Evans, *J. Electrochem. Soc.* **136**, 819 (1989).
- ²⁶R. A. Svehla, Nasa Technical Report TR R-B2, 1962.
- ²⁷D. A. Doughty and A. Gallagher, *Phys. Rev. A* **42**, 6166 (1990).
- ²⁸J. M. Jasinski and J. O. Chu, *J. Chem. Phys.* **88**, 1678 (1988); J. O. Chu, D. B. Beach, R. D. Estes, and J. M. Jasinski, *Chem. Phys. Lett.* **143**, 135 (1988).
- ²⁹D. B. Beach and J. M. Jasinski, *J. Phys. Chem.* **94**, 3019 (1990).
- ³⁰P. Haaland, Ph.D. thesis, Harvard University, 1988.
- ³¹M. L. Mandich, W. D. Reents, Jr., and K. D. Kolenbranden, *J. Chem. Phys.* **92**, 437 (1990).
- ³²M. L. Mandich and W. D. Reents, Jr., *J. Chem. Phys.* **90**, 3121 (1989).
- ³³M. L. Mandich, W. D. Reents, Jr., and M. F. Jarrold, *J. Chem. Phys.* **88**, 1703 (1988).
- ³⁴E. R. Fisher and P. B. Armentrout, *J. Chem. Phys.* **93**, 4858 (1990).
- ³⁵H. Chatham, D. Hils, R. R. Robertson, and A. C. Gallagher, *J. Chem. Phys.* **79**, 1301 (1983).
- ³⁶H. Chatham, D. Hils, R. Robertson, and A. Gallagher, *J. Chem. Phys.* **81**, 1770 (1984).
- ³⁷H. Yoshida, Y. Moishima, M. Ukai, K. Shinsaka, N. Kouchi, and Y. Hatono, *Chem. Phys. Lett.* **176**, 173 (1991).
- ³⁸M. Tsuji, K. Kobarai, S. Yamaguchi, and Y. Nishimura, *Chem. Phys. Lett.* **158**, 470 (1989).
- ³⁹M. Tsuji, K. Kobarai, S. Yamaguchi, H. Obase, K. Yamaguchi, and Y. Nishimura, *Chem. Phys. Lett.* **155**, 481 (1989).
- ⁴⁰J. L. Jouberteau, D. Conte, M. I. Baratron, P. Quintard, J. Aubreton, and A. Catherinot, *Plasma Chem. Plasma Proc.* **10**, 401 (1990).
- ⁴¹D. F. Davidson, K. Kohse-Hoinghaus, A. Y. Chang, and R. K. Hanson, *Int. J. Chem. Kinet.* **22**, 513 (1990).
- ⁴²D. B. Peterson, US Department of Commerce, Report NSRDS-NBS 44, 1974.
- ⁴³D. L. Albritton, *At. Data Nucl. Data Tables* **22**, 8 (1978).
- ⁴⁴I. Haller, *J. Phys. Chem.* **94**, 4135 (1990).
- ⁴⁵L. E. Kline, *IEEE Trans. Plasma Sci.* **PS-10**, 24 (1982).
- ⁴⁶D. L. Smith, A. S. Alimonda, C.-C. Chen, S. E. Ready, and B. Wacker, *J. Electrochem. Soc.* **137**, 614 (1990).
- ⁴⁷T. Fuyuki, B. Allain, and J. Perrin, *J. Appl. Phys.* **68**, 3322 (1990).
- ⁴⁸D. L. Smith, A. S. Alimonda, and F. J. von Preissig, *J. Vac. Sci. Technol. B* **8**, 551 (1990).
- ⁴⁹J. Batey, E. Tierney, J. Stasiak, and T. N. Nguyen, *Appl. Surf. Sci.* **39**, 1 (1989).
- ⁵⁰P. Boher, J. Schneider, M. Renaud, Y. Hily, and J. Bruines, *J. Appl. Phys.* **66**, 3410 (1990).
- ⁵¹J. M. S. Henis, G. W. Stewart, M. K. Tripodi, and P. P. Gaspar, *J. Chem. Phys.* **57**, 389 (1972).
- ⁵²H. Chatham and A. Gallagher, *J. Appl. Phys.* **58**, 159 (1985).
- ⁵³T.-Y. Yu, T. M. H. Cheng, V. Kenpter, and F. W. Lampe, *J. Phys. Chem.* **76**, 3321 (1972).
- ⁵⁴W. Hack, P. Rouveiolles, and H. G. Wagner, *J. Chem. Phys.* **90**, 2505 (1986).
- ⁵⁵C. Zetzsch and F. Stuhl, *Ber. Bunsenges. Phys. Chem.* **85**, 864 (1981).
- ⁵⁶A. W. Boyd, C. Willis, and O. A. Miller, *Can. J. Chem.* **49**, 2283 (1971).
- ⁵⁷S. Gordon, W. Mulac, and P. Nangia, *J. Phys. Chem.* **75**, 2087 (1971).
- ⁵⁸M. Demissy and R. Leschaux, *J. Am. Chem. Soc.* **102**, 2897 (1980).
- ⁵⁹P. Khe, J. C. Soullignac, and R. Leschoux, *J. Phys. Chem.* **81**, 210 (1977).
- ⁶⁰J. Dove and S. W. Nip, *Can. J. Chem.* **57**, 689 (1979).
- ⁶¹C. Mori, *Symp. Int. Combust. Proc.* **18**, 13 (1981).
- ⁶²J. Balamuta, M. F. Golde, and Y.-S. Ho, *J. Chem. Phys.* **79**, 2822 (1983).
- ⁶³P. A. Jerram and A. C. H. Smith, *J. Phys. B* **18**, 1747 (1985).
- ⁶⁴T. D. Mark, in *Electron Impact Ionization*, edited by T. D. Mark and G. H. Dunn (Springer, Vienna, 1985), p. 144.
- ⁶⁵For example, see J. Perrin and T. Broekhuizen, *Appl. Phys. Lett.* **50**, 433 (1987).